Feedback inhibition by a descending GABAergic neuron regulates timing of escape behavior in *Drosophila* larvae

Jiayi Zhu[1,2], Jean-Christophe Boivin[1,2], Alastair Garner[1,2], Jing Ning[1], Yi Qing Zhao[1], Tomoko Ohyama[1,2,3*]

[1] Department of Biology, McGill University, Docteur Penfield Ave., Montreal, QC, H3A 1B1, Canada
[2] Integrated Program of Neuroscience, Pine Ave. W., McGill University, Montreal, QC, H3A 1A1, Canada
[3] Alan Edwards Center for Research on Pain, McGill University, University St., Montreal, QC, H3A 2B4, Canada

*Correspondence: tomoko.ohyama@mcgill.ca

Keywords: escape behavior, nociceptive circuit, descending neuron, GABA, *Drosophila*

Abstract

Escape behaviors help animals avoid harm from predators and other threats in the environment. Successful escape relies on integrating information from multiple stimulus modalities (of external or internal origin) to compute trajectories toward safe locations, choose between actions that satisfy competing motivations, and execute other strategies that ensure survival. To this end, escape behaviors must be adaptive. When a *Drosophila melanogaster* larva encounters a noxious stimulus, such as the focal pressure a parasitic wasp applies to the larval cuticle via its ovipositor, it initiates a characteristic escape response. The escape sequence consists of an initial abrupt bending, a corkscrew-like rolling, and finally rapid crawling. Previous work has shown that the detection of noxious stimuli primarily relies on class IV multi dendritic arborization neurons (Class IV neurons) located beneath the body wall, and more recent studies have identified several important components in the nociceptive neural circuitry involved in rolling. However, the neural mechanisms that underlie the rolling-escape sequence remain unclear. Here we present both functional and anatomical evidence suggesting that bilateral descending neurons within the

subesophageal zone of *D. melanogaster* larva play a crucial role in regulating the termination of rolling and subsequent transition to escape crawling. We demonstrate that these descending neurons (designated SeIN128) are inhibitory and receive inputs from a second-order interneuron upstream (Basin-2) and an ascending neuron downstream of Basin-2 (A00c). Together with optogenetic experiments showing that co-activation of SeIN128 neurons and Basin-2 influence the temporal dynamics of rolling, our findings collectively suggest that the ensemble of SeIN128, Basin-2, and A00c neurons forms a GABAergic feedback loop onto Basin-2, which inhibits rolling and thereby facilitates the shift to escape crawling.

Introduction

Virtually all organisms on earth face the threat of being maimed or killed by one or more predatory organisms. Not surprisingly, when organisms encounter threat-associated stimuli, they exhibit a wide variety of escape responses appropriate to their biological construction and the specific predators within their ecological niche (Burrell, 2017; Campagner et al., 2023; Chin & Tracey, 2017; Im & Galko, 2012; Peirs & Seal, 2016). Typically, these escape responses consist of a sequence of simple actions. The roundworm *C. elegans*, for example, in response to a touch to its head, exhibits rapid backward locomotion coupled with a suppression of head movements, followed by a deep ventral bend (omega turn) and a 180-degree reversal in the direction of locomotion. This sequence allows the roundworm to escape from nematophagal fungi that cohabitate with it in organic debris (Chalfie & Sulston, 1981; Chalfie et al., 1985).

When *Drosophila melanogaster* larvae encounter noxious stimuli, such as the stimulation that accompanies an attempt by a parasitic wasp to penetrate the larval cuticle with its ovipositor, they exhibit an escape response consisting of an initial abrupt bending, followed by corkscrew-like rolling, and finally, rapid crawling (Hwang et al., 2007; Ohyama et al., 2015; Onodera et al., 2017; Tracey et al., 2003). Previous work has shown that noxious stimuli are primarily detected by class IV dendritic arborization neurons (Class IV neurons) located beneath the body wall (Tracey et al., 2003). More recent studies have identified several important components in the downstream nociceptive neural circuitry, particularly those involved in rolling (Burgos et al., 2018; Dason et al., 2020; Hu et al., 2017; Hu et al., 2020; Imambocus et al., 2022; Kaneko et al., 2017; Ohyama et al., 2015; Takagi et al., 2017; Yoshino et al., 2017). To date, however, the neural mechanisms

that underlie the rolling-escape sequence, notably, the transition from rolling to crawling, have remained unclear.

In this study, we provide both functional and anatomical evidence that, bilateral descending neurons in the subesophageal zone (SEZ) of *D. melanogaster* larva, which comprise part of a neural circuit underlying rolling, a characteristic nocifensive escape response, potentially regulate the termination of rolling and subsequent transition to escape crawling. We show that these descending neurons, which we designate as SeIN128, are identical to those denoted previously as SS04185 (Ohyama et al., 2015), are inhibitory neurons that receive inputs from Basin-2 (a second-order interneuron upstream) and A00c (an ascending neuron downstream of Basin-2), and provide GABAergic feedback onto Basin-2. Together with behavioral analyses of rolling during systematic optogenetic manipulation of SeIN128 and Basin-2 activity, our findings suggest that an ensemble of neurons—SeIN128, Basin-2, and A00c—forms an inhibitory feedback circuit that inhibits rolling, which in turn facilitates the shift to escape crawling.

SS04185 facilitates rolling termination and shortens the latency of crawling behavior in the escape responses

In a previous study, we showed that activation of all Basin neurons (Basin-1, -2, -3, and -4) induced rolling followed by fast crawling (Figure 1A–D) (Ohyama et al., 2015). Here, we first examined whether optogenetic activation of all four Basins expressing the red-shifted opsin CsChrimson (using Basin-1-4 Gal4, i.e., R72F11-Gal4) could elicit the same behavior. Upon activation of all Basins, we observed rolling mostly within the first 5 s, followed by crawling (Figure 1B (top panel), C and D). The crawling speed during activation of all Basins following rolling was ~1.5 times that of the crawling speed at baseline (Figure 1D) (Ohyama et al., 2015).

To identify the neurons responsible for escape behavior (rolling and/or fast crawling), we conducted a behavioral screening of ~250 split Gal4 lines that were labeled in the central nervous system (CNS) when co-activated with all Basins. With respect to rolling, we found that activation of the split-Gal4 line, SS04185 (i.e., w^{1118}; *R54B01-Gal4*^{AD}; *R46E07-Gal4*^{DBD}), significantly reduced the probability of rolling when compared to activating only the Basins (Figure 1B, C, E, Video 1 and 2) without affecting the crawling speed during stimulation (Figure 1D).

The likelihood of rolling upon co-activation of SS04185 neurons and Basins might decrease because activation of SS04185 neurons trigger other actions, such as crawling, head casting,

hunching, or stopping, and not because they solely inhibit rolling evoked by Basins. To investigate this possibility, we examined the effect of activating only SS04185 and found that this did not induce any extra actions such as crawling, turning, hunching, or stopping (Figure 1–figure supplement 1A-D). These data suggest that co-activation of Basins and SS04185 neurons reduces rolling because SS04185 activation inhibits the Basin circuit.

Next, we explored how the quality of rolling changed during co-activation of SS04185 and Basin neurons. First, we examined the amount of time animals spent rolling during Basin activation. The average time spent rolling (percentage of the 30-s stimulation period) was 23.9% (7.2 s out of 30 s) following activation of Basins alone, whereas it was only 5.9% following co-activation of Basins and SS04185 (1.8 s out of 30 s) (Figure 1–figure supplement 1E). Additionally, the duration of each rolling bout was significantly shorter when SS04185 neurons were co-activated with Basins (Mann-Whitney U test, $p < 0.001$; Figure 1F).

The duration of a rolling bout could decrease because of changes in the latency to initiate rolling, latency to terminate rolling, or both. To investigate how SS04185 activation affects these temporal parameters of rolling, we analyzed the latencies for the initiation and termination of the first rolling bout. Compared to activating Basins alone, co-activating the Basins and SS04185-expressing neurons only marginally increased latency to onset of the first rolling bout (Figure 1G), whereas it markedly reduced the latency for the termination of rolling (Mann-Whitney U test, $p < 0.001$; Figure 1H). These data strongly suggest that SS04185-expressing neurons are involved in terminating rolling.

If the rolling module inhibits crawling, then premature termination of rolling might allow crawling to commence sooner than normal. Co-activation of SS04185 and Basins resulted in the initiation of the first crawling bout occurring earlier than when only Basins were activated (Mann Whitney U test, $p < 0.001$; Figure 1I, Figure 1–figure supplement 1F). The time from the end of rolling to the start of crawling remained similar between the groups in which the Basins were activated alone and in which the Basins and SS04185 were co-activated (Figure 1–figure supplement 1G). This is consistent with the higher probability of crawling during activation of SS04185 and Basin neurons (Figure 1–figure supplement 1H). Lastly, activation of SS04185 neurons in conjunction with Basins did not change the crawling speed compared to activation of Basins alone (Figure 1–figure supplement 1I). These results collectively indicate that SS04185 activation terminates rolling and facilitates the shift to fast crawling.

127

128 **A pair of descending neurons in SS04185 contributes to termination of rolling**

129 To identify the neurons that express SS04185 upon CsChrimson activation, we examined the
130 localization of SS04185-labeled neurons. We found that SS04185 split-Gal4 strongly labeled a
131 pair of descending neurons located within the subesophageal zone (SEZ) and mushroom body
132 (MB) neurons within the brain (Figure 2A). To pinpoint which of these neurons are involved in
133 reducing the probability of rolling (Figure 1B, C and E), we varied the level of SS04185 expression
134 among the pair of SS04185-expressing descending neurons (SS04185-DN) and the SS04185-
135 expressing MB (SS04185-MB) neurons (jointly with the Basins as in Figure 1). These
136 manipulations allowed us to assess the resultant behavioral outcomes.

137 If SS04185-MB neurons are involved in the modulation of rolling, then reducing SS04185-MB
138 expression should reduce the extent to which activation of both SS04185-DN neurons and
139 SS04185-MB neurons decreases the probability of rolling. To test this conjecture, we expressed
140 Killer Zipper ($KZip^{+}$), which interferes with the binding of $Gal4^{AD}$ and $Gal4^{DBD}$ in SS04185-MB
141 neurons with MB LexA line (R13F02-LexA), consequently leading to a significant reduction in
142 CsChrimson expression in SS04185-MB neurons (Figure 2B, Figure 2–figure supplement 1A)
143 (Dolan et al., 2017; Vogt et al., 2016). When compared to $KZip^{+}$ controls, which do not express
144 SS04185 (Figure 2C, black bars), however, activation of SS04185 neurons with reduced SS04185-
145 MB expression (Figure 2C, red bars on the right; Figure 2–figure supplement 1B) still reduced
146 rolling probability (as well as the total duration of rolling [Figure 2–figure supplement 1C]) to a
147 level no different from that of $KZip^{-}$ controls expressing SS04185 fully in both SS04185-MB and
148 SS04185-DN neurons (Figure 2C, dark red bars in the middle). Additionally, co-activation of MB
149 Gal4 lines (MB247-Gal4) with Basins (without activation of SS04185-DN neurons) did not reduce
150 the probability of rolling (Figure 2–figure supplement 1D-E) (Pauls et al., 2010). These data
151 indicate that SS04185-DN neurons inhibit rolling.

152 To further test the role of SS04185-DN neurons, we investigated whether these neurons were
153 involved in reducing the duration of each rolling bout (Figure 1A, D and F). As a result, knockdown
154 of SS04185-MB neurons did not increase the duration of rolling bouts (Figure 2D). Furthermore,
155 the earlier onset of crawling triggered by the activation of SS04185 neurons remained the same
156 with knockdown of SS04185-MB neurons (Figure 2E). Collectively, these results strongly suggest

that the behavioral effects on both rolling and crawling, as illustrated in Figure 1, are primarily mediated by SS04185-DN neurons.

To further ascertain the role of SS04185-DN neurons in the regulation of rolling, we employed the heat shock FlpOut mosaic expression approach. This technique allowed for controlled and sporadic expression of CsChrimson in SS04185 neurons thorough random induction of Flippase by manipulating the timing and duration of heat shock (Golic and Lindquist, 1989; Nern et al., 2015). We compared larvae subjected to activation of both SS04185-MB and SS04185-DN neurons (red, Figure 2–figure supplement 1F) with those subjected only to activation of SS04185-MB neurons (black, Figure 2–figure supplement 1G), to assess the degree to which the former showed behavioral effects. Remarkably, activation of both SS04185-MB and SS04185-DN neurons resulted in a reduction in both the probability and duration of rolling when compared to activation of SS04185-MB neurons alone (Figure 2F and G, Figure 2–figure supplement 1H-I). Furthermore, activation of both SS04185-MB and SS04185-DN neurons reduced the latency to the end of the first rolling bout and the initiation of the first crawling bout (Figure 2H, Figure 2–figure supplement 1J). These findings provide compelling evidence that SS04185-DN neurons, but not SS04185-MB neurons, play an important role in the termination of rolling. Collectively, the results suggest that a single pair of descending neurons in SS04185 is important for termination of rolling during the activation of Basins.

Descending neurons identified by SS04185 correspond to SeIN128 neurons

In a previous EM study, we identified a set of neurons designated as SeIN128, whose cell bodies in the SEZ send axonal projections throughout the thoracic and abdominal segments (Figure 3A) (Ohyama et al., 2015). Our immunostaining data also showed that the cell bodies of SS04185-DN neurons are located in the SEZ, with axons bilaterally innervating the medial regions of the ventral nerve cord (VNC) from the thoracic to abdominal segments A8/9 (Figure 2A), suggesting that SS04185-DN and SeIN128 neurons are one and the same.

To verify this possibility, we examined the detailed anatomy of SS04185-DN neurons by immunostaining them with several markers and compared our immunostaining images with the corresponding images obtained via EM reconstruction of the entire CNS of a 1st instar *Drosophila* larva (Ohyama et al., 2015; Winding et al., 2023). We confirmed that the projections of SeIN128 neurons are distributed within the ventromedial neural tract (one of the six major neural tracts) in

188 *Drosophila* larvae (Figure 3A, B, and C) in EM reconstruction data. We also confirmed that the
189 cell bodies of SS04185-DN neurons were again located in the SEZ region, where the most anterior
190 of the three neuropils in the thoracic region was marked by N-cadherin (Figure 3D). Viewed from
191 the side (i.e., in the longitudinal or sagittal plane), both the cell bodies and axonal arbor were
192 located ventrally (Figure 3D, far right). Immunostaining with Fasciclin2 (Fas2), which labels
193 various neural tracts in the VNC (Grenningloh et al., 1991; Santos et al., 2007), showed
194 colocalization of the axonal projections of SS04185-DN neurons and the Fas2-labeled
195 ventromedial tract (Figure 3C and E). The similarity of the locations of their cell bodies and the
196 distributions of their axonal processes suggests the identity of the SS04185-DN and SeIN128
197 neurons.
198 A previous EM study showed that SeIN128 neurons were located downstream of Basin neurons
199 (Ohyama et al., 2015). To further confirm the identity of SS04185-DN and SeIN128 neurons, we
200 compared the distributions of the axonal projections of SS04185-DN neurons in relation to those
201 of several key neurons within the rolling circuit: the Basins, A00c neurons (a group of ascending
202 neurons downstream of the Basins, and which facilitate rolling), and mdIV neurons (nociceptive
203 sensory neurons upstream of the Basins). Immunostaining revealed that Basin projections
204 colocalize with those of SS04185-DN neurons in both the horizontal and transverse planes (Figure
205 3F, top and lower panels, respectively), with the horizontal view showing that SS04185-DN
206 projections are distributed slightly medial to those of Basins within the ventromedial tract (Figure
207 3F, top panels), which resembles their colocalization pattern reported in EM (Figure 3B, C and G).
208 Similarly, we compared the distributions of SS04185-DN projections with those of A00c or mdIV
209 projections. We found that the projections of A00c colocalize with those of SS04185-DN in a
210 similar fashion along the rostrocaudal axis within the ventromedial tract (Figure 3H and I), with
211 A00c projections distributed more medially than SS04185-DN projections, consistent with the
212 distribution patterns of SeIN128 projections and A00c projections in the EM reconstruction dataset
213 (Figure 3B, H and I). In contrast, the distributions of mdIV projections did not colocalize with
214 those of SS04185-DN projections, as the mdIV projections were displaced more laterally relative
215 to the SS04185-DN projections in the horizontal and transverse planes (Figure 3J, top and lower
216 panels, respectively), consistent with the distribution patterns of SeIN128 and mdIV projections in
217 the EM reconstruction dataset (Figure 3K). In the transverse plane, the projections of SS04185-
218 DN neurons were also distributed dorsomedial to those of mdIV (Figure 3J, lower panel),

consistent with the corresponding distribution patterns in the EM reconstruction dataset (Figure 3B, C and K).

We conclude that the morphological findings for SS04185-DN neurons, together with data on the distribution of their axonal projections in relation to that of Basin, A00c, and mdIV neurons, strongly suggest the identity of SS04185-DN and SeIN128 neurons.

Connectome and functional connectivity analyses: SeIN128 neurons receive inputs from Basin-2 and A00c

A previous study that reconstructed larval neurons involved in the rolling circuit showed that Basin-2 and A00c neurons (in the VNC) make excitatory synaptic contacts onto SeIN128 neurons (in the CNS), which in turn make reciprocal inhibitory synaptic contacts onto Basin-2 and A00c neurons (Figure 4A, Figure 4–figure supplement 1A) (Ohyama et al., 2015). These data suggest that SeIN128 neurons are directly activated by Basin-2 and A00c (which also receives inputs from Basin-1, Basin-2, and Basin-4).

To assess the functional significance of these synaptic connections between SeIN128 neurons and Basins or A00c, we activated either Basins or A00c neurons and examined the resultant GCaMP signaling in SeIN128 neurons. Specifically, after expressing CsChrimson in Basins and A00c neurons and GCaMP in SeIN128 neurons, we used a two-photon microscope (920-nm laser) and monitored GCaMP signaling in SeIN128 neurons during illumination of a specimen with a 620-nm LED for 1 s (0.04–1.4 $\mu W/mm^2$), which activated either Basins or A00c neurons. GCaMP signals in SeIN128 neurons increased in an intensity-dependent manner when either Basins and A00c were activated (Figure 4B and C) but not when larvae were not fed retinal (Figure 4–figure supplement 1C and D). Peak activity occurred at around 3 s after the onset of LED stimulation, which was similar to the results when Basins or A00c neurons were stimulated (Figure 4B and C). Finally, both Basin and A00c stimulation resulted in linear dose-dependent increases in SeIN128 firing (Figure 4–figure supplement 1B). These results are consistent with the notion that SeIN128 neurons are downstream of Basins and A00c neurons.

To compare the neural responses between Basins and SeIN128 or A00c neurons, we recorded neural activity in A00c neurons with GCaMP while stimulating Basin neurons in the same experimental setting. Although A00c neurons displayed a similar dose-dependent increase in peak axonal firing as the intensity of optogenetic stimulation of Basin neurons increased, unlike

250 SeIN128 neurons they showed no delay in peak firing activity (Figure 4D and E, Figure 4–figure
251 supplement 1B), suggesting that A00c and SeIN128 neurons function differently in the rolling
252 circuit.
253 We then investigated the anatomical locations of the synaptic outputs and inputs of SeIN128
254 neurons, and found that, whereas their outgoing projections primarily make synaptic contacts
255 along the anterior-posterior nerve axis, the inputs coming from other neurons are mainly located
256 in the SEZ (Figure 3A). On the other hand, SeIN128 neurons make axo-axonal contacts onto
257 Basin-2 neurons (Figure 4–figure supplement 2A-G) as well as A00c neurons: that is, their axons
258 make synaptic contacts with the dorsal and medial processes of Basin-2, which correspond to their
259 axonal compartments (Figure 4–figure supplement 2E-G). These data suggest that the delay of
260 SeIN128 activity may be caused by multi-synaptic connections involving the SEZ or a feedback
261 loop involving axo-axonal connections between SeIN128 and Basin-2 or A00c.
262
263 **SeIN128 neurons are GABAergic and inhibitory**
264 The results thus far indicate that, activation of SeIN128 neurons inhibits rolling (Figure 1A–C);
265 SeIN128 neurons receive functional inputs from Basin-2 and A00c (Figure 4A-C); and SeIN128
266 neurons make anatomical connections onto Basin-2 and A00c (Figure 4A). These findings suggest
267 that SeIN128 neurons might be inhibitory. To test this possibility, we performed immunostaining
268 experiments and found that SeIN128 neurons colocalized with glutamic acid decarboxylase (Gad)-
269 positive neurons but not with acetylcholine- or glutamate-positive neurons, suggesting that
270 SeIN128 neurons are GABAergic inhibitory neurons (Figure 5A, Figure 5–figure supplement 1A,
271 and B).
272 We reasoned that if GABA in SeIN128 neurons is necessary for inhibiting rolling, then selectively
273 knocking down GABA secretion in SeIN128 neurons should enhance rolling. When we expressed
274 RNAi *HMS02355* in SeIN128 neurons to knock down vesicular GABA transporter (VGAT)
275 expression and suppress the release of GABA, the population-level rolling probability increased
276 from 23.6% to 45.2% (Figure 5B and C) (Kallman et al., 2015; Zhao et al., 2019). We confirmed
277 the effect of *HMS02355* by immunostaining: pan-neural *HMS02355* expression decreased GABA
278 and VGAT expression in the neuropil (Figure 5–figure supplement 1C, and D). The control group
279 (only Basins expressing CsChrimson with VGAT RNAi HMS02355 but without SS04185) showed
280 a lower probability of rolling (23.6%) compared to similar genotypes without VGAT RNAi

281 HMS02355 (Figure 2C, F). This indicates that VGAT RNAi HMS02355 background reduces the
282 probability of rolling. Furthermore, the duration of each bout of rolling increased from 0.8 s to 1.4
283 s (Figure 5D). These data support the idea that SeIN128 neurons inhibit rolling via GABAergic
284 transmission.
285
286 **Inhibition of SeIN128 increases probability and duration of rolling**
287 To further test whether the release of GABA upon activating SeIN128 neurons is necessary for
288 inhibiting rolling, we expressed tetanus toxin (TNT) in SeIN128 neurons to block synaptic
289 transmission. Silencing SeIN128 neurons via TNT while triggering rolling by optogenetically
290 activating Basin neurons via *R72F11-LexA>LexAop-CsChrimson* significantly increased the
291 probability of rolling compared to controls (Figure 6A and B). Silencing SeIN128 neurons via
292 TNT extended the duration of each rolling bout, as well as the total rolling duration, in each larva
293 (Figure 6C and D). We also examined the rolling-escape crawling sequence upon silencing
294 SeIN128 neurons, and found that the time to offset of rolling and the time onset of crawling were
295 both delayed relative to controls (Figure 6E and F).
296 Given that TNT is expressed constitutively during development, long-term compensatory changes
297 in the nervous system could have contributed to alterations in the parameters of rolling and
298 crawling. To test whether similar results could be replicated with the use of a temporally specific
299 intervention, we expressed *shibire*^{ts1} (*shi*^{ts1}) in SeIN128 neurons to block synaptic transmission at
300 temperatures above 30°C (van de Goor et al., 1995; Kitamoto, 2001). Silencing SeIN128 neurons
301 via *shibire*^{ts1} increased the probability of rolling from 60.4% to 79.7% (Figure 6–figure supplement
302 1A and B). The total duration of rolling per animal during stimulation increased from 10 to 12 s
303 (Figure 6–figure supplement 1C). Although the duration of each rolling bout, the time to onset of
304 the first rolling bout, and time to onset of the first crawling bout did not differ from those of
305 controls (Figure 6–figure supplement 1D, E and G), the time to offset of the first rolling bout was
306 delayed relative to controls ($p = 0.013$ for Figure 6–figure supplement 1F). Together with the
307 results showing that activation of SeIN128 neurons inhibits rolling, these findings suggest that the
308 activity of SeIN128 neurons is important in controlling the duration of rolling and the shift to
309 crawling.
310
311 **Basins receive GABAergic inputs that inhibit rolling**

312 Given that Basins receive axo-axonal inputs from SeIN128 neurons and GABA signaling in
313 SeIN128 neurons inhibits rolling, we next used RNA interference (RNAi) to test whether Basins
314 receive GABAergic signals from SeIN128. We hypothesized that knockdown of GABA receptors
315 in Basin neurons would increase the probability and duration of rolling at the population level. To
316 knock down ionotropic GABA-A receptors (GABA-A-R) and G-protein-coupled GABA-B
317 receptors (GABA-B-R1 and GABA-B-R2), we tested Basin neurons with GABA-A-R, GABA-B-
318 R1, and GABA-B-R2 RNAi lines (i.e., *HMC03643* for GABA-A-R, *HMC03388* for GABA-B-
319 R1[1], *JF02989* for GABA-B-R1[2] and *HMC02975* for GABA-B-R2, respectively). For all RNAi
320 lines, the rolling probability at the population level increased from 80% to 90% or even higher
321 (Figure 7A), while the total rolling duration at the individual level increased for each larva
322 throughout the stimulation window (Figure 7–figure supplement 1A). All GABA receptor
323 knockdown groups showed significant increases in rolling duration across multiple bouts (Figure
324 7B); all groups except for GABA-B-R1[1] showed a reduced time to onset of the first rolling bout
325 (Figure 7–figure supplement 1B); and only the GABA-B-R2 and GABA-A-R groups showed a
326 delayed offset of the first rolling bout (Figure 7–figure supplement 1C). None of the groups
327 differed from controls in the time to onset of the first crawling bout (Figure 7–figure supplement
328 1D). The greatest increase in the probability and duration of rolling was seen during knockdown
329 of ionotropic GABA-A-R (*Rdl*), suggesting that Rdl contributes most to the inhibition of Basin
330 neurons (Figure 7A and B).
331 To investigate whether SeIN128 neurons actually inhibit Basins, we recorded the activity of all
332 Basins during activation of SeIN128 neurons. We compared GCaMP signaling in the Basins when
333 they were co-activated with SeIN128 neurons (experimental treatment) or when they were
334 activated alone (control treatment), with the intensity of optogenetic stimulation varied from 0.04
335 to 1.4 $\mu W/mm^2$. We found that Basins in the experimental group showed reductions in GCaMP
336 signaling by 11% to 36% compared to those in the control group (Figure 7C, Figure 7–figure
337 supplement 1E and F). The reductions were observed at all stimulation intensities when contrasting
338 peak GCaMP responses, and statistically significant at intensities of 0.3 and 0.5 $\mu W/mm^2$ (Figure
339 7C, Figure 7–figure supplement 1E and F). Collectively, these data support the idea that SeIN128
340 neurons directly inhibit the activity of Basins via GABA.
341
342 **Effects of SeIN128 activation on rolling elicited by activating individual Basins**

In the studies above, we measured the activity of all Basins while manipulating the activity of SeIN128 neurons. Connectome and behavioral analyses indicate, however, that of the four types of Basins, only Basin-2 and Basin-4 receive nociceptive input from mdIV and trigger rolling (Ohyama et al., 2015). Moreover, as noted above, an examination of the larval connectome (Ohyama et al., 2015; Winding et al., 2023) revealed that Basin-2 both receives axo-axonal inputs from SeIN128 neurons and sends excitatory projections to the same SeIN128 neurons, whereas a similar examination revealed that Basin-4 neither receives inputs from, nor sends any outputs to, SeiN128 neurons. Therefore, we hypothesized that activation of SeIN128 neurons would inhibit rolling elicited by Basin-2 activation and modify the temporal parameters of rolling, but not affect rolling elicited by Basin-4 activation.

We first examined the pattern of rolling evoked by optogenetically activating Basin-2. Basin-2 activation induced multiple bouts of rolling throughout the stimulation window (Figure8–figure supplement 1A). Furthermore, the rolling elicited by Basin-2 activation tended to be sustained (Figure8–figure supplement 1A). Next, to determine how SeIN128 activation affects the pattern of rolling elicited by Basin-2 activation, we optogenetically activated SeIN128 neurons and Basin-2 simultaneously. As expected, compared to the probability of rolling in control animals in which only Basin-2 was activated, the probability of rolling in experimental animals in which Basin-2 and SeIN128 neurons were simultaneously activated was significantly lower (66.7% vs 24.4%; Figure 8A, Figure 8–figure supplement 1D). We also examined other parameters of rolling, including the time from the start (onset) of stimulation to the onset of the first rolling bout, termination (offset) of the first rolling bout, and onset of the first crawling bout, as well as the duration of the rolling bout (i.e., the time from its onset to its offset). Consistent with the hypothesis that SeIN128 activation inhibits Basin-2 activity, the duration of the rolling bout significantly decreased (Figure 8B, Mann-Whitney U test, $p = 0.0034$, *Cohen's d* = 0.351) and the time to onset of the first rolling bout significantly increased in experimental animals compared to controls (Figure 8–figure supplement 1E; Mann-Whitney U test, $p < 0.001$). In addition, as expected, the time to offset of the first rolling bout (Figure 8C; Mann-Whitney U test, $p = 0.0047$, *Cohen's d* = 0.607) and time to onset of the first crawling bout (Figure 8D; Mann-Whitney U test, $p = 0.0074$, *Cohen's d* = 0.548) both significantly decreased in experimental animals compared to controls. Collectively, these findings suggest that Basin-2 neurons play a major role in mediating the effects of SeIN128 activation on rolling induced by optogenetic activation of all Basin neurons.

To ascertain our expectation that SeIN128 activation would have little if any effect on the pattern of rolling elicited by Basin-4 activation, given the absence of any identifiable synaptic contacts between Basin-4 neurons and SeIN128 neurons based on available information on the larval connectome, we also carried out the same analyses as those described above for rolling elicited by Basin-2 activation. We examined the pattern of rolling evoked by optogenetically activating Basin-4, and found that this manipulation induced rolling mostly within the first 5 s of stimulation (Figure 8–figure supplement 1B and F). Consequently, at the population level, rolling elicited by Basin-4 activation was transient compared to the rolling elicited by Basin-2 activation (compare Figure 8–figure supplement 1A vs 1B) (Figure 8–figure supplement 1C).

We then assessed whether SeIN128 activation would affect rolling elicited by Basin-4 activation. Surprisingly, compared to control animals, the probability of rolling in experimental animals was significantly lower (66.7% vs 26.8%; Figure 8E), much as was the case for rolling elicited by Basin-2 activation. We also examined the other rolling parameters, and found that the duration of the rolling bouts (Figure 8F; Mann-Whitney U test, $p = 0.032$, *Cohen's d = 0.248*), time to offset of the first rolling bout (Figure 8G; Mann-Whitney U test, $p < 0.0047$, *Cohen's d = 0.427*), and time to onset of the first crawling bout (Figure 8H; Mann-Whitney U test, $p < 0.001$, *Cohen's d = 1.039*) all significantly decreased in experimental animals compared to controls, although the effect sizes were smaller compared to those observed for rolling elicited by Basin-2 activation. The time to onset of the first rolling bout, however, did not significantly differ between experimental animals and controls (Figure 8–figure supplement 1G). These findings suggest the possibility that sites further downstream of Basin-4 neurons may be involved in inhibitory processes that affect rolling elicited by Basin-4 activation.

Discussion

In this study, we provide both anatomical and functional evidence that, bilateral descending neurons in the brain of *D. melanogaster* larva, which comprise part of a neural circuit underlying a characteristic rolling response that larvae exhibit when evading parasitization by wasps, potentially regulates the termination of rolling and the subsequent transition to escape crawling. We showed that these descending neurons, which we designated as SeIN128, were identical to those previously identified as a component of the nociceptive circuit; were inhibitory neurons that receive excitatory inputs from Basin-2, a second-order interneuron upstream, and A00c, an

405 ascending neuron downstream of Basin-2; and provided GABAergic feedback onto Basin-2,
406 presumably via the axo-axonal synaptic contacts made by the axon terminal endings of SeIN128
407 neurons onto the axons of Basin-2. Optogenetic activation studies further showed that co-
408 activation of SeIN128 and Basin-2 neurons systematically altered the temporal dynamics of rolling
409 and subsequent escape crawling. Collectively, the evidence suggests that the ensemble of SeIN128,
410 Basin-2, and A00c neurons constitutes a novel inhibitory feedback circuit provides reduces Basin-
411 2 activity. This, in turn, influence the activity of a key interneuron of the rolling circuit via a novel
412 inhibitory mechanism.

413 **Feedback inhibition in a nociceptive circuit**

414 Feedback inhibition occurs when an excitatory neuron sends projections to an inhibitory neuron,
415 which in turn sends projections back onto the same excitatory neuron, often at its presynaptic
416 terminals (Isaacson & Scanziani, 2011; Kapfer et al., 2007; Ray et al., 2020; Stokes & Isaacson,
417 2010; Yoshimura & Callaway, 2005). The hallmark of feedback inhibition lies in its ability to
418 modulate the duration and magnitude of incoming excitatory signals, thereby fine-tuning neural
419 responses and maintaining homeostasis (Kapfer et al., 2007; Papadopoulou et al., 2011; Stokes &
420 Isaacson, 2010; Yoshimura & Callaway, 2005). Compared to the fast temporal dynamics of
421 feedforward inhibition, in which an inhibitory neuron directly inhibits an excitatory neuron
422 downstream of it, the temporal dynamics of feedback inhibition are slower, primarily due to the
423 added synaptic delays (two or more) following activation of an excitatory neuron (Papadopoulou
424 et al., 2011; Ray et al., 2020; Stokes & Isaacson, 2010). The slow temporal dynamics serve to
425 inhibit the sustained neural activity and magnitude of incoming excitatory signals (Papadopoulou
426 et al., 2011; Ray et al., 2020; Stokes & Isaacson, 2010).

427 In this study, we showed that SeIN128 neurons are descending neurons whose main inputs arrive
428 in the brain and SEZ regions, and whose outputs target the VNC. We also found that SeIN128
429 neurons receive excitatory inputs from Basin-2 as well as its downstream neuron A00c, and in turn
430 send inhibitory projections back to these neurons in the VNC, potentially establishing a feedback
431 inhibition motif that modulates the nociceptive rolling circuit. The interplay we observed among
432 SeIN128 neurons, Basin-2, and A00c is consistent with this view. Our findings revealed that
433 activation of SeIN128 neurons has a suppressive effect on Basin-2 activity and, notably, on the
434 duration of rolling. These observations support the idea that feedback inhibition is critical in
435 regulating the temporal aspects of nociceptive responses.

436 **Inhibition of Basin-2 by SeIN128 neurons is mediated by axo-axonal synapses**

437 Neurons form a wide variety of neural networks that perform various computations in the brain.
438 Typically, a neuron receives inputs via axo-dendritic synapses (i.e., contacts made by the axon
439 terminals of an upstream neuron with its dendrites), which play a role in the spatial and temporal
440 computations that lead to the firing of action potentials. Less commonly, the axon terminals of an
441 upstream neuron may contact the soma (i.e., via axo-somatic synapses) or axon (i.e., via axo-
442 axonal synapses) of a downstream neuron (Palay, 1956; Pinault et al., 1997; Zheng et al., 2018).
443 Axo-axonal synapses have a subtle effect on neurotransmission at the network level because the
444 activity in presynaptic neurons does not alter the membrane potential (Cattaert & El Manira, 1999;
445 Guo & Hu, 2014; McGann, 2013). Axo-axonal synapses mainly affect the release probability of
446 neurotransmitter vesicles in response to an action potential triggered in the postsynaptic neuron
447 (McGann, 2013; Oleson et al., 2012).

448 Recent studies suggest that the activity of axo-axonal synapses can prevent the transmission of
449 action potentials. For example, it has been reported that, neurotransmission mediated by type-B
450 muscarinic receptors at lateral axo-axonal connections between *Drosophila* Kenyon Cells is
451 critical for stimulus specificity learning in *Drosophila* (Manoim et al., 2022); inhibitory axo-axonal
452 connections between Chandelier cells and CA1 pyramidal cells are important for activity-
453 dependent plasticity (Pan-Vazquez et al., 2020; Schneider-Mizell et al., 2021); and GABAergic
454 axo-axonal interneurons in the amygdala are crucial for generating action potentials in the principal
455 output cells (Veres et al., 2023). Furthermore, EM connectome analyses of the entire larval brain
456 reveal that ~70% of all synapses in *Drosophila* larvae are axo-dendritic whereas ~30% are axo-
457 axonal, suggesting that the latter may have considerable influence over network function (Winding
458 et al., 2023).

459 In this study, we found a feedback connection between SeIN128 and Basin-2 mediated by axon-
460 axonal synapses (Figure 4–figure supplement 2E-G). The slow increase of SeIN128 activity in
461 response to Basin-2 or A00c activation could potentially occur because of these axo-axonal
462 connections. Alternatively, the slow response in SeIN128 may involve an as yet unidentified
463 indirect connections from Basin-2 or A00c to the main inputs in the SEZ region. This delayed
464 activity may play an important role in the feedback inhibition of Basin-2 activity and consequently
465 in the termination of rolling.

466 **Role of SeIN128 in other escape behaviors**

467 Although the current study focused on rolling, activation of SS04185 neurons appeared to
468 influence other escape behaviors. First, *during* co-activation of SS04185 and Basins (Figure 1B,
469 lower panel), the frequency of crawling following the initial rolling bout increased compared to
470 when only the Basins were activated in which animals typically showed multiple rolling bouts
471 during the 30-s stimulation period (Figure 1B, upper panel). This observation might be attributed
472 to the strong stimulation induced by Chrimson activation of Basins alone that interrupts crawling
473 via the intrusion of repeated rolling bouts, compared with the co-activation of SS04185 neurons
474 and Basins that reduces the intrusion of rolling. More notably, *after* either co-activation of SS04185
475 neurons and Basins (Figure 1B, lower panel) or activation of SS04185 neurons alone (data not
476 shown), the frequency of turning increased *upon the cessation (offset) of stimulation*, but not
477 following the activation of basins alone (Figure 1B, upper panel). This second observation suggests
478 the possibility that activation of SS04185 neurons leads to sustained inhibition of turning
479 throughout the stimulation period, which when released upon the offset of stimulation, results in a
480 rebound in the frequency of turning beyond baseline levels. Alternatively, activation of SS04185-
481 MB neurons alone may independently trigger the increase in turning frequency following the offset
482 of stimulation (Figure 1B, Figure 2–figure supplement 1K). A comprehensive examination of this
483 question, however, is beyond the scope of the present study.

484 **Roles of Basin-2 and Basin-4 in escape behavior**

485 Previous studies have shown that, Basin-2 and Basin-4 receive both chordotonal sensory and
486 nociceptive sensory inputs, and in addition, play a critical role in escape behavior (Ohyama et al.,
487 2015). Here we investigated the differences between rolling induced by activation of Basin-2 or
488 Basin-4. We found that activation of Basin-2 induced rolling that was sustained. Furthermore,
489 activation of SeIN128 neurons reduced the duration of rolling induced by co-activation of Basin-
490 2, which resulted in a delay in the onset of rolling and an earlier termination of rolling. These data
491 indicate that activation of Basin-2 serves to maintain rolling. Connectome data indicate that
492 SeIN128 neurons provide inhibitory input onto Basin-2, which is consistent with the finding that
493 SeIN128 activation reduces the duration of rolling.

494 On the other hand, activation of Basin-4 induced rolling that was transient, which was then
495 followed by rapid crawling. Furthermore, activation of SeIN128 neurons reduced the probability
496 of rolling but did not affect the duration of rolling (Figure 8F). This suggests that activation of
497 Basin-4 is important for the induction of rolling, but not its maintenance. The behavioral effects of

498 coactivating SeIN128 and Basin-4, together with connectome data indicating the lack of
499 connections between SeIN128 neurons and Basin-4, suggest that these descending neurons target
500 neurons downstream of Basin-4 neurons.

501 **Other inputs onto SeIN128 neurons modify escape behavior**

502 The dendritic regions of SeIN128 neurons are located in the SEZ and brain, suggesting that
503 SeIN128 neurons receive other inputs from the SEZ and brain neurons. In this study, we did not
504 examine these inputs. Connectome data indicate that MB output neurons project onto SeIN128
505 neurons (Ohyama et al., 2015). Given the well-established role of MB neurons in learning, this
506 finding suggests that SeIN128 neurons could play a role in experience-dependent modulation of
507 rolling. Two recent studies have shown that descending neurons inhibit nociceptive neurons
508 (Nakamizo-Dojo et al., 2023; Oikawa et al., 2023). Specifically, one study showed that insulin
509 signaling modulates escape behavior by activating GABAergic descending neurons that inhibit
510 nociceptive sensory neurons (Nakamizo-Dojo et al., 2023), whereas the other demonstrated an
511 inhibitory mechanism mediated by the neuropeptide Drosulfakinin, a homologue of
512 cholecystokinin in mammals (Oikawa et al., 2023). Whether SeIN128 neurons are also influenced
513 by insulin signaling or Drosulfakinin, however, remains to be seen.

514 **Implications for mechanistic analyses of behavioral sequences**

515 In this study, we did not investigate how crawling is initiated after rolling. Recent studies of the
516 motor circuits underlying rolling and crawling suggest that different premotor neurons are involved
517 in driving each action (Cooney et al., 2023; Kohsaka, 2023; Zarin et al., 2019). When we co-
518 activated SS04185 and Basins, the duration of rolling decreased and the latency to onset of
519 crawling decreased. These data are consistent with the notion that the rolling circuit inhibits the
520 crawling circuit. It would be of interest examine if premotor crawling neurons are inhibited during
521 rolling, and if so, how they are activated following Basin inhibition to trigger crawling.

522

523 In summary, our study delineates a neuronal ensemble consisting of a set of descending inhibitory
524 neurons, a first-order interneuron (Basin-2), and an ascending neuron (A00c) in fruit fly larvae,
525 which functions as an inhibitory feedback circuit that regulates the probability and duration of
526 rolling, and thereby facilitates the transition from rolling to crawling. This work represents another
527 example of how detailed analyses of connectomes and functional analyses of neural and behavioral

528 activity can identify mechanistic explanations of behavioral phenomena at the level of neural
529 circuits—in this case, how neuronal ensembles generate behavioral sequences.
530

531 **Materials and Methods:**

532 **Key resources table**

Reagent or resource	Source or reference	Identifiers
Antibodies		
Mouse anti-Brp monoclonal antibody, clone nc82	Developmental Studies Hybridoma Bank	Cat# nc82, RRID:AB_2314866
Mouse 1D4 anti-fasciclin II antibody	Developmental Studies Hybridoma Bank	Cat# 1D4 anti-Fasciclin II, RRID:AB_528235
Rat anti-cadherin, DN- (extracellular domain) antibody	Developmental Studies Hybridoma Bank	Cat# DN-Ex #8, RRID:AB_528121
Chicken anti-GFP antibody	Abcam	Cat# ab13970, RRID:AB_300798
Rabbit anti-GFP polyclonal antibody, unconjugated	Thermo Fisher Scientific	Cat# A-6455, RRID:AB_221570
Rabbit anti-DsRed polyclonal antibody	Takara Bio	Cat# 632496, RRID:AB_10013483
Mouse anti-Drosophila choline acetyltransferase monoclonal antibody, unconjugated	Developmental Studies Hybridoma Bank	Cat# chat4b1, RRID:AB_528122
Rabbit anti-GABA antibody	Millipore Sigma	Cat # A2052
Rabbit anti-Drosophila VGLUT antibody	Gift from McCabe lab	Ref: (Banerjee et al., 2021)
Rabbit anti-VGAT antibody	Gift from Krantz lab	Ref: (Fei et al., 2010)
Rat anti-Elav antibody	Developmental Studies Hybridoma Bank Gift from Aberbe lab	Cat# 7E8A10, RRID:AB_528218
Goat anti-chicken IgY (H+L) secondary antibody, Alexa Fluor™ 488	Thermo Fisher Scientific	Cat# A-11039, RRID:AB_2534096
Goat anti-rabbit IgG (H+L) highly cross-adsorbed secondary antibody, Alexa Fluor™ 488	Thermo Fisher Scientific	Cat# A-11034, RRID:AB_2576217
Goat anti-rabbit IgG (H+L) cross-adsorbed secondary antibody, Alexa Fluor™ 568	Thermo Fisher Scientific	Cat# A-11011, RRID:AB_143157
Goat anti-mouse IgG (H+L) cross-adsorbed secondary antibody, Alexa Fluor™ 568	Thermo Fisher Scientific	Cat# A-11004, RRID:AB_2534072
Goat anti-rat IgG (H+L) Alexa Fluor™ 568	Thermo Fisher Scientific	Cat# A-11077, RRID:AB_2534121
Chemicals		
PBS, Phosphate Buffered Saline, 10x solution	Fisher Scientific	Cat# BP399-1
Triton X-100	Millipore Sigma	Cat# X100-100ML
Paraformaldehyde 20% aqueous solution	Electron Microscopy Sciences	Cat# 15713
Normal goat serum	Gibco	PCN5000
VECTASHIELD antifade mounting medium	Vector Laboratories	Cat# H-1000-10
Drosophila Agar	Diamed	Cat# GEN66-103
All Trans Retinal	Toronto Research Chemicals Inc.	Cat# R24000
Poly-L-lysine	Sigma-Aldrich	Cat# P1524
Fly strains		

R72F11-Gal4 (attp2)	Bloomington Drosophila Stock Center	RRID: BDRC_39786
R71A10-Gal4 (attp2)	Bloomington Drosophila Stock Center	RRID: BDRC_39562
w; R54B01-Gal4^{AD};R46E07-Gal4^{DBD} (SS04185)	Gift from Zlatic lab	N/A
w; R72F11-Gal4^{AD};R38H09-Gal4^{DBD} (SS00739)	Gift from Zlatic lab	N/A
w; R72F11-Gal4^{AD};R57F07-Gal4^{DBD} (SS00740)	Gift from Zlatic lab	N/A
MB247-Gal4, mef2-Gal4	Bloomington Drosophila Stock Center	RRID: BDRC_50742
R13F02-LexA (attp40)	Bloomington Drosophila Stock Center	RRID: BDRC_52460
R72F11-LexA (attp40)	Bloomington Drosophila Stock Center	RRID: BDRC_94661
R71A10-LexA (attp40)	Gift from Zlatic lab	N/A
Mi{Trojan-LexA-QFAD.2}Gad1	Bloomington Drosophila Stock Center	RRID: BDRC_60324
20xUAS-IVS-CsChrimson::mVenus (attp2)	Bloomington Drosophila Stock Center	RRID: BDRC_55134
20xUAS-IVS-CsChrimson::mVenus (attP18)	Bloomington Drosophila Stock Center	RRID: BDRC_55136
20xUAS-IVS-CsChrimson::mVenus (attP18);;R72F11-Gal4 (attp2)	Bloomington Drosophila Stock Center	RRID: BDRC_79599
13xLexAop2-IVS-CsChrimson::mVenus (attP18)	Bloomington Drosophila Stock Center	RRID: BDRC_55137
13xLexAop2-IVS-CsChrimson::tdTomato (attP18)	Gift from Rubin lab	N/A
13xLexAop2-IVS-CsChrimson::tdTomato (vk000005)	Bloomington Drosophila Stock Center	RRID: BDRC_82183
20xUAS(FRT.stop)CsChrimson.mVenus(attP18), pBPhsFlp2::Pest (AttP3)	Gift from Rubin lab	N/A
hs(KDRT.stop)FLP (attP18)	Bloomington Drosophila Stock Center	RRID: BDRC_67091
20xUAS(FRT.stop)-CsChrimson::mVenus	Gift from Rubin lab	N/A
UAS-TeTxLC.tnt	Bloomington Drosophila Stock Center	RRID: BDRC_28838
20xUAS-TTS-Shibire^{ts1}-p10(vk00005)	Bloomington Drosophila Stock Center	PRID: BDRC_66600
10xUAS-IVS-mry::GFP (attP18)	Gift from Rubin lab	N/A
13xLexAop-dsRed (attP2)	Gift from Rubin lab	N/A
20xUAS-IVS-GCaMP6s (vk00005)	Bloomington Drosophila Stock Center	RRID: BDRC_4279
20xLexAop-IVS-Syn21-GCaMP6s (su(HW)attP8)	Gift from Rubin lab	N/A
20xUAS-Syn21-opGCaMP6s (su(Hw)attP8)	Gift from Rubin lab	N/A
10xUAS-Syn21-CsChrimson88::tdTomato(attP18)	Gift from Rubin lab	N/A
HMS02355	Bloomington Drosophila Stock Center	RRID: BDRC_41958
HMC03388	Bloomington Drosophila Stock Center	RRID: BDRC_51817
JF02989	Bloomington Drosophila Stock Center	RRID: BDRC_28353
HMC02975	Bloomington Drosophila Stock Center	RRID: BDRC_50608
HMC03643	Bloomington Drosophila Stock Center	RRID: BDRC_52903
Software and algorithms		

FIJI	https://fiji.sc/	RRID: SCR_002285
MATLAB	MathWorks	RRID: SCR_001622
CATMAID	https://catmaid.readthe docs.org/	RRID: SCR_006278
Multi Worm Tracker	http://sourceforge.net/projects/mwt	N/A
ZEN	Carl Zeiss Microscopy	Version 2.1 (blue edition)
Affinity Designer	Affinity	Version 1.10.5
ScanImage	MBF Bioscience	N/A

533

534 **Fly stocks and maintenance**

535 All *D. melanogaster* stock lines used in this study were raised on Bloomington Drosophila Stock
536 Center cornmeal food. Flies were maintained in a humidity- and temperature-controlled chamber
537 kept at 18°C or 25°C, 40% humidity, and set to a 12-hour light/dark cycle. All crosses for
538 experiments were reared at 25°C and 40% humidity.

539 **Heat shock FlpOut mosaic expression**

540 First instar *Drosophila* larvae were heat shocked in water bath at 37°C for 12 min as previously
541 reported (Nern et al., 2015). With the precise temporal and temperature control of heat shock,
542 larvae with the genotype of w^{+}, *hs(KDRT.stop)FLP/13xLexAop2-IVS-CsChrimson::tdTomato;*
543 *R54B01-Gal4.AD/72F11-LexA;20xUAS-(FRT.stop)-CsChrimson::mVenus/R46E07-Gal4.DBD*
544 had sporadic CsChrimson::mVenus expression driven by SS04185 split GAL4. As a result, the
545 ratio of the larvae with SS04185-DN and SS04185-MB expression to those with only SS04185-
546 MB expression was 1:1. Each individual larva was individually examined with optogenetic
547 stimulation and behavior analysis. After behavioral experiments, mVenus expression in CNS was
548 confirmed under the fluorescence microscope.

549 **Fly genotypes used in experiments**

550 **-Main figures**

Fig.	Panel	Labels	Genotypes
1	B	Basins>Chrimson	*20xUAS-IVS-CsChrimson::mVenus/+;+; R72F11-Gal4/+*
1	B	Basins + SS04185>Chrimson	*20xUAS-IVS-CsChrimson::mVenus/+; R54B01-Gal4.AD/+; R46E07-Gal4.DBD/ R72F11-Gal4*
1	C-D, F	control	*20xUAS-IVS-CsChrimson::mVenus/+; +; R72F11-Gal4/+*
1	C-D, F	SS04185	*20xUAS-IVS-CsChrimson::mVenus/+; R54B01-Gal4.AD/+; R46E07-Gal4.DBD/R72F11-Gal4*
1	E	ctrl / attp2>Chrimson	*20xUAS-IVS-CsChrimson::mVenus/+;;*
1	E	SS04185 / attp2>Chrimson	*20xUAS-IVS-CsChrimson::mVenus/+; R54B01-Gal4.AD/+; R46E07-Gal4.DBD/+*
1	E	ctrl / Basins>Chrimson	*20xUAS-IVS-CsChrimson::mVenus/+; +; R72F11-Gal4/+*
1	E	SS04185 / Basins>Chrimson	*20xUAS-IVS-CsChrimson::mVenus/+; R54B01-Gal4.AD/+; R46E07-Gal4.DBD/R72F11-Gal4*
1	G-I	ctrl	*20xUAS-IVS-CsChrimson::mVenus/+; +; R72F11-Gal4/+*
1	G-I	SS04185	*20xUAS-IVS-CsChrimson::mVenus/+; R54B01-Gal4.AD/+; R46E07-Gal4.DBD/R72F11-Gal4*
2	A		*10xUAS-IVS-myr::GFP/+; R54B01-Gal4.AD/+; R46E07-Gal4.DBD/+*

2	B	control	*20xUAS-IVS-CsChrimson::mVenus/+; R54B01-Gal4.AD/+; R46E07-Gal4.DBD/R72F11-Gal4*
2	B	MB>KZip+	*20xUAS-IVS-CsChrimson::mVenus/+; R13F02-LexA,LexAop-KZip^{+}/R54B01-Gal4.AD; R72F11-Gal4/R46E07-Gal4.DBD*
2	C, E	MB>KZip+ / ctrl	*20xUAS-IVS-CsChrimson::mVenus/+; R13F02-LexA,LexAop-KZip^{+}/+; R72F11-Gal4/+*
2	C, E	- / SS04185	*20xUAS-IVS-CsChrimson::mVenus/+; R54B01-Gal4.AD/+; R46E07-Gal4.DBD/R72F11-Gal4*
2	C, E	MB>KZip+ / SS04185	*20xUAS-IVS-CsChrimson::mVenus/+; R13F02-LexA,LexAop-KZip^{+}/R54B01-Gal4.AD; R72F11-Gal4/R46E07-Gal4.DBD*
2	D	MB>KZip+	*20xUAS-IVS-CsChrimson::mVenus/+; R13F02-LexA,LexAop-KZip^{+}/+; R72F11-Gal4/+*
2	D	SS04185	*20xUAS-IVS-CsChrimson::mVenus/+; R54B01-Gal4.AD/+; R46E07-Gal4.DBD/R72F11-Gal4*
2	D	MB>KZip+, SS04185	*20xUAS-IVS-CsChrimson::mVenus/+; R13F02-LexA,LexAop-KZip^{+}/R54B01-Gal4.AD; R72F11-Gal4/R46E07-Gal4.DBD*
2	F, H	ctrl	*w+, hs(KDRT.stop)FLP/13xLexAop2-IVS-CsChrimson::tdTomato; R54B01-Gal4.AD/72F11-LexA;20xUAS-(FRT.stop)-CsChrimson::mVenus/R46E07-Gal4.DBD*
2	F, H	SS04185-DN	*w+, hs(KDRT.stop)FLP/13xLexAop2-IVS-CsChrimson::tdTomato; R54B01-Gal4.AD/72F11-LexA;20xUAS-(FRT.stop)-CsChrimson::mVenus/R46E07-Gal4.DBD*
2	G	control	*w+, hs(KDRT.stop)FLP/13xLexAop2-IVS-CsChrimson::tdTomato; R54B01-Gal4.AD/72F11-LexA;20xUAS-(FRT.stop)-CsChrimson::mVenus/R46E07-Gal4.DBD*
2	G	SS04185-DN	*w+, hs(KDRT.stop)FLP/13xLexAop2-IVS-CsChrimson::tdTomato; R54B01-Gal4.AD/72F11-LexA;20xUAS-(FRT.stop)-CsChrimson::mVenus/R46E07-Gal4.DBD*
3	D, E		*10xUAS-IVS-myr::GFP/+; R54B01-Gal4.AD/+; R46E07-Gal4.DBD/+*
3	F		*w; R54B01-Gal4.AD/R72F11-LexA; R46E07-Gal4.DBD/13xLexAop2-IVS-CsChrimson::tdTomato, 20xUAS-IVS-GCaMP6s*
3	H		*w; R54B01-Gal4.AD/R71A10-LexA; R46E07-Gal4.DBD/13xLexAop2-IVS-CsChrimson::tdTomato, 20xUAS-IVS-GCaMP6s*
3	J		*w; R54B01-Gal4.AD/ppk1.9-LexA; R46E07-Gal4.DBD/13xLexAop2-IVS-CsChrimson::tdTomato, 20xUAS-IVS-GCaMP6s*
4	B		*w; R72F11-LexA/R54B01-Gal4.AD; 13xLexAop-CsChrimson, 20xUAS-IVS-UAS-GCaMP6s/R46E07-Gal4.DBD*
4	C		*w; R71A10-LexA/R54B01-Gal4.AD; 13xLexAop-CsChrimson, 20xUAS-IVS-UAS-GCaMP6s/R46E07-Gal4.DBD*
4	D		*w; R72F11-LexA/+; 13xLexAop2-IVS -CsChrimson::tdTomato, 20xUAS-IVS-UAS-GCaMP6s/R71A10-Gal4*
4	E	A00c	*w; R72F11-LexA/+; 13xLexAop2-IVS -CsChrimson::tdTomato, 20xUAS-IVS-UAS-GCaMP6s/R71A10-Gal4*
4	E	SS04185	*w; R72F11-LexA/R54B01-Gal4.AD; 13xLexAop2-IVS -CsChrimson::tdTomato, 20xUAS-IVS-UAS-GCaMP6s/R46E07-Gal4.DBD*
5	A		*10xUAS-myr::GFP; R54B01-Gal4.AD/13x-LexAop-dsRed; R46E07-Gal4.DBD/ Mi{Trojan-LexA-QFAD.2}Gad1*
5	B, D	control	*13xLexAop2-IVS-CsChrimson::mVenus;R72F11-lexA/+; HMS02355/+*
5	B, D	SS04185	*13xLexAop2-IVS-CsChrimson::mVenus; R72F11-lexA/R54B01-Gal4.AD; HMS02355/R46E07-Gal4.DBD*
5	C	ctrl	*13xLexAop2-IVS-CsChrimson::mVenus;R72F11-lexA/+; HMS02355/+*
5	C	SS04185	*13xLexAop2-IVS-CsChrimson::mVenus; R72F11-lexA/R54B01-Gal4.AD; HMS02355/R46E07-Gal4.DBD*
6	A	control>TNT	*13xLexAop2-IVS-CsChrimson::mVenus; R72F11-LexA/+; UAS-TeTxLC.tnt /+*
6	A	SS04185>TNT	*13xLexAop2-IVS-CsChrimson::mVenus; R72F11-LexA/R54B01-Gal4.AD; UAS-TeTxLC.tnt/R46E07-Gal4.DBD*
6	B, D-F	ctrl	*13xLexAop2-IVS-CsChrimson::mVenus; R72F11-LexA/+; UAS-TeTxLC.tnt /+*
6	B, D-F	SS04185	*13xLexAop2-IVS-CsChrimson::mVenus; R72F11-LexA/R54B01-Gal4.AD; UAS-TeTxLC.tnt/R46E07-Gal4.DBD*
6	C	control	*13xLexAop2-IVS-CsChrimson::mVenus; R72F11-LexA/+; UAS-TeTxLC.tnt /+*
6	C	SS04185	*13xLexAop2-IVS-CsChrimson::mVenus; R72F11-LexA/R54B01-Gal4.AD; UAS-TeTxLC.tnt/R46E07-Gal4.DBD*
7	A, B	control	*20xUAS-IVS-CsChrimson::mVenus/+; ; R72F11-Gal4/+*
7	A, B	GABA-B-R1[1]	*20xUAS-IVS-CsChrimson::mVenus/+; ; R72F11-Gal4/UAS-HMC03388*
7	A, B	GABA-B-R1[2]	*20xUAS-IVS-CsChrimson::mVenus/+; ; R72F11-Gal4/UAS-JF02989*
7	A, B	GABA-B-R2	*20xUAS-IVS-CsChrimson::mVenus/+; ; R72F11-Gal4/UAS-HMC02975*

7	A, B	GABA-A-R	*20xUAS-IVS-CsChrimson::mVenus/+; ; R72F11-Gal4/UAS-HMC03643*
7	C	control	*20xUAS-Syn21-opGCaMP6s,10xUAS-Syn21-CsChrimson88::tdTomato/+;CyO/+;TM6/R72F11-Gal4*
7	C	SS04185	*20xUAS-Syn21-opGCaMP6s,10xUAS-Syn21-CsChrimson88::tdTomato/+;CyO/R54B01-Gal4.AD;R72F11-Gal4/R46E07-Gal4.DBD*
8	A, C-D	ctrl	*20xUAS-IVS-CsChrimson::mVenus/+; R72F11-Gal4.AD/+; R38H09-Gal4.DBD/+*
8	A, C-D	SS04185	*20xUAS-IVS-CsChrimson::mVenus/+; R72F11-Gal4.AD/R54B01-Gal4.AD; R38H09-Gal4.DBD/R46E07-Gal4.DBD*
8	B	control	*20xUAS-IVS-CsChrimson::mVenus/+; R72F11-Gal4.AD/+; R38H09-Gal4.DBD/+*
8	B	SS04185	*20xUAS-IVS-CsChrimson::mVenus/+; R72F11-Gal4.AD/R54B01-Gal4.AD; R38H09-Gal4.DBD/R46E07-Gal4.DBD*
8	E, G-H	ctrl	*20xUAS-IVS-CsChrimson::mVenus/+; R72F11-Gal4.AD/+; R57F07-Gal4.DBD/+*
8	E, G-H	SS04185	*20xUAS-IVS-CsChrimson::mVenus/+; R72F11-Gal4.AD/R54B01-Gal4.AD; R57F07-Gal4.DBD/R46E07-Gal4.DBD*
8	F	control	*20xUAS-IVS-CsChrimson::mVenus/+; R72F11-Gal4.AD/+; R57F07-Gal4.DBD/+*
8	F	SS04185	*20xUAS-IVS-CsChrimson::mVenus/+; R72F11-Gal4.AD/R54B01-Gal4.AD; R57F07-Gal4.DBD/R46E07-Gal4.DBD*

-Supplementary figures

Fig.	Panel	Labels	Genotypes
1-1	A-D	ctrl	*20xUAS-IVS-CsChrimson::mVenus/+;;*
1-1	A-D	SS04185	*20xUAS-IVS-CsChrimson::mVenus/+; R54B01-Gal4.AD/+; R46E07-Gal4.DBD/+*
1-1	E, G-H	ctrl	*20xUAS-IVS-CsChrimson::mVenus/+; +; R72F11-Gal4/+*
1-1	E, G-H	SS04185	*20xUAS-IVS-CsChrimson::mVenus/+; R54B01-Gal4.AD/+; R46E07-Gal4.DBD/R72F11-Gal4*
1-1	F	control	*20xUAS-IVS-CsChrimson::mVenus/+; +; R72F11-Gal4/+*
1-1	F	SS04185	*20xUAS-IVS-CsChrimson::mVenus/+; R54B01-Gal4.AD/+; R46E07-Gal4.DBD/R72F11-Gal4*
1-1	I	ctrl / attp2>Chrimson	*20xUAS-IVS-CsChrimson::mVenus/+;;*
1-1	I	SS04185 / attp2>Chrimson	*20xUAS-IVS-CsChrimson::mVenus/+; R54B01-Gal4.AD/+; R46E07-Gal4.DBD/+*
1-1	I	ctrl / Basins>Chrimson	*20xUAS-IVS-CsChrimson::mVenus/+; +; R72F11-Gal4/+*
1-1	I	SS04185 / Basins>Chrimson	*20xUAS-IVS-CsChrimson::mVenus/+; R54B01-Gal4.AD/+; R46E07-Gal4.DBD/R72F11-Gal4*
1-2	A-C	control	*20xUAS-IVS-CsChrimson::mVenus/+;; R72F11-Gal4/+*
1-2	A-C	54B01-AD	*20xUAS-IVS-CsChrimson::mVenus/+; R54B01-Gal4.AD/+; R72F11-Gal4/+*
1-2	A-C	46E07-DBD	*20xUAS-IVS-CsChrimson::mVenus/+; +; R72F11-Gal4/ R46E07-Gal4.DBD*
1-2	A-C	SS04185	*20xUAS-IVS-CsChrimson::mVenus/+; R54B01-Gal4.AD/+; R46E07-Gal4.DBD/R72F11-Gal4*
2	A		*20xUAS-IVS-CsChrimson::mVenus/+; R13F02-LexA,LexAop-KZip^{+}/R54B01-Gal4.AD; R72F11-Gal4/R46E07-Gal4.DBD*
2	B	MB>Kzip+	*20xUAS-IVS-CsChrimson::mVenus/+; R13F02-LexA,LexAop-Kzip^{+}/+; R72F11-Gal4/+*
2	B	SS04185	*20xUAS-IVS-CsChrimson::mVenus/+; R54B01-Gal4.AD/+; R46E07-Gal4.DBD/R72F11-Gal4*
2	B	MB>Kzip+, SS04185	*20xUAS-IVS-CsChrimson::mVenus/+; R13F02-LexA,LexAop-Kzip^{+}/R54B01-Gal4.AD; R72F11-Gal4/R46E07-Gal4.DBD*
2	C	MB>Kzip+ / ctrl	*20xUAS-IVS-CsChrimson::mVenus/+; R13F02-LexA,LexAop-Kzip^{+}/+; R72F11-Gal4/+*
2	C	- / SS04185	*20xUAS-IVS-CsChrimson::mVenus/+; R54B01-Gal4.AD/+; R46E07-Gal4.DBD/R72F11-Gal4*
2	C	MB>Kzip+ / SS04185	*20xUAS-IVS-CsChrimson::mVenus/+; R13F02-LexA,LexAop-Kzip^{+}/R54B01-Gal4.AD; R72F11-Gal4/R46E07-Gal4.DBD*
2	D	control	*20xUAS-IVS-CsChrimson::mVenus/+; +; R72F11-Gal4/+*
2	D	MB247	*20xUAS-IVS-CsChrimson::mVenus/+; R54B01-Gal4.AD/+; R46E07-Gal4.DBD/R72F11-Gal4*
2	E	ctrl	*20xUAS-IVS-CsChrimson::mVenus/+; +; R72F11-Gal4/+*
2	E	MB247	*20xUAS-IVS-CsChrimson::mVenus/+; R54B01-Gal4.AD/+; R46E07-Gal4.DBD/R72F11-Gal4*

2	F, G		*w+, hs(KDRT.stop)FLP/13xLexAop-CsChrimson::tdTomato; R54B01-Gal4.AD/72F11-LexA;20xUAS-(FRT.stop)-CsChrimson::mVenus/R46E07-Gal4.DBD*
2	H	control	*w+, hs(KDRT.stop)FLP/13xLexAop-CsChrimson::tdTomato; R54B01-Gal4.AD/72F11-LexA; 20xUAS-(FRT.stop)-CsChrimson::mVenus/R46E07-Gal4.DBD*
2	H	SS04185-DN	*w+, hs(KDRT.stop)FLP/13xLexAop-CsChrimson::tdTomato; R54B01-Gal4.AD/72F11-LexA; 20xUAS-(FRT.stop)-CsChrimson::mVenus/R46E07-Gal4.DBD*
2	I-J	ctrl	*w+, hs(KDRT.stop)FLP/13xLexAop-CsChrimson::tdTomato; R54B01-Gal4.AD/72F11-LexA; 20xUAS-(FRT.stop)-CsChrimson::mVenus/R46E07-Gal4.DBD*
2	I-J	SS04185-DN	*w+, hs(KDRT.stop)FLP/13xLexAop-CsChrimson::tdTomato; R54B01-Gal4.AD/72F11-LexA; 20xUAS-(FRT.stop)-CsChrimson::mVenus/R46E07-Gal4.DBD*
4	B	Basins>Chrimson	*w; R72F11-LexA/R54B01-Gal4.AD; 13xLexAop2-IVS -CsChrimson::tdTomato, 20xUAS-IVS- GCaMP6s/R46E07-Gal4.DBD*
4	B	A00c>Chrimson	*w; R71A10-LexA/R54B01-Gal4.AD; 13xLexAop2-IVS -CsChrimson::tdTomato, 20xUAS-IVS-GCaMP6s/R46E07-Gal4.DBD*
4	C	SeIN128 (Basins>Chrimson)	*w; R72F11-LexA/R54B01-Gal4.AD; 13xLexAop2-IVS -CsChrimson::tdTomato, 20xUAS-IVS- GCaMP6s/R46E07-Gal4.DBD*
4	C	SeIN128 (A00c>Chrimson)	*w; R71A10-LexA/R54B01-Gal4.AD; 13xLexAop2-IVS -CsChrimson::tdTomato, 20xUAS-IVS-GCaMP6s/R46E07-Gal4.DBD*
4	C	A00c (Basins>Chrimson)	*w; R72F11-LexA/+; 13xLexAop2-IVS -CsChrimson::tdTomato, 20xUAS-IVS-GCaMP6s/R71A10-Gal4*
5	A, B		*10xUAS-IVS-myr::GFP/+; R54B01-Gal4.AD/+; R46E07-Gal4.DBD/+*
5	C, D	ctrl	*w; ; R57C10-Gal4/+*
5	C, D	VGAT-RNAi	*w; ; R57C10-Gal4/UAS-HMS02355*
6	A, D	control	*13xLexAop2-IVS-CsChrimson::mVenus; R72F11-LexA/+; 20xUAS-TTS-Shibire^{ts1}/+*
6	A, D	SS04185	*13xLexAop2-IVS-CsChrimson::mVenus; R72F11-LexA/R54B01-Gal4.AD; 20xUAS-TTS-Shibire^{ts1}/R46E07-Gal4.DBD*
6	B-C, E-G	ctrl	*13xLexAop2-IVS-CsChrimson::mVenus; R72F11-LexA/+; 20xUAS-TTS-Shibire^{ts1}/+*
6	B-C, E-G	SS04185	*13xLexAop2-IVS-CsChrimson::mVenus; R72F11-LexA/R54B01-Gal4.AD; 20xUAS-TTS-Shibire^{ts1}/R46E07-Gal4.DBD*
7	A-D	control	*20xUAS-IVS-CsChrimson::mVenus/+; ; R72F11-Gal4/+*
7	A-D	GABA-B-R1[1]	*20xUAS-IVS-CsChrimson::mVenus/+; ; R72F11-Gal4/UAS-HMC03388*
7	A-D	GABA-B-R1[2]	*20xUAS-IVS-CsChrimson::mVenus/+; ; R72F11-Gal4/UAS-JF02989*
7	A-D	GABA-B-R2	*20xUAS-IVS-CsChrimson::mVenus/+; ; R72F11-Gal4/UAS-HMC02975*
7	A-D	GABA-A-R	*20xUAS-IVS-CsChrimson::mVenus/+; ; R72F11-Gal4/UAS-HMC03643*
7	E	Basins>Chrimson	*20xUAS-Syn21-opGCaMP6s,10xUAS-Syn21-CsChrimson88::tdTomato/+;CyO/+;TM6/R72F11-Gal4*
7	F	Basins + SeIN128>Chrimson	*20xUAS-Syn21-opGCaMP6s,10xUAS-Syn21-CsChrimson88::tdTomato/+;CyO/R54B01-Gal4.AD;R72F11-Gal4/R46E07-Gal4.DBD*
8	A	Basin2>Chrimson	*20xUAS-IVS-CsChrimson::mVenus/+; R72F11-Gal4.AD/+; R38H09-Gal4.DBD/+*
8	B	Basin4>Chrimson	*20xUAS-IVS-CsChrimson::mVenus/+; R72F11-Gal4.AD/+; R57F07-Gal4.DBD/+*
8	C	Basin-2	*20xUAS-IVS-CsChrimson::mVenus/+; R72F11-Gal4.AD/+; R38H09-Gal4.DBD/+*
8	C	Basin-4	*20xUAS-IVS-CsChrimson::mVenus/+; R72F11-Gal4.AD/+; R57F07-Gal4.DBD/+*
8	D	control	*20xUAS-IVS-CsChrimson::mVenus/+; R72F11-Gal4.AD/+; R38H09-Gal4.DBD/+*
8	D	SS04185	*20xUAS-IVS-CsChrimson::mVenus/+; R72F11-Gal4.AD/R54B01-Gal4.AD; R38H09-Gal4.DBD/R46E07-Gal4.DBD*
8	E	ctrl	*20xUAS-IVS-CsChrimson::mVenus/+; R72F11-Gal4.AD/+; R38H09-Gal4.DBD/+*
8	E	SS04185	*20xUAS-IVS-CsChrimson::mVenus/+; R72F11-Gal4.AD/R54B01-Gal4.AD; R38H09-Gal4.DBD/R46E07-Gal4.DBD*
8	F	control	*20xUAS-IVS-CsChrimson::mVenus/+; R72F11-Gal4.AD/+; R57F07-Gal4.DBD/+*
8	F	SS04185	*20xUAS-IVS-CsChrimson::mVenus/+; R72F11-Gal4.AD/R54B01-Gal4.AD; R57F07-Gal4.DBD/R46E07-Gal4.DBD*
8	G	ctrl	*20xUAS-IVS-CsChrimson::mVenus/+; R72F11-Gal4.AD/+; R57F07-Gal4.DBD/+*
8	G	SS04185	*20xUAS-IVS-CsChrimson::mVenus/+; R72F11-Gal4.AD/R54B01-Gal4.AD; R57F07-Gal4.DBD/R46E07-Gal4.DBD*

Behavior assay

554 To optogenetically stimulate neurons, embryos were collected for 24 hours and larvae were raised
555 on fly food plates with 0.2 mM trans-retinal (Toronto Research Chemicals, R240000). The larvae
556 were kept in the dark at 25°C for four days to grow to the 3rd instar stage. Before the experiment,
557 food plates with larvae were rinsed with a 15% sucrose solution to separate the larvae from the
558 food. Larvae were then moved to a sieve, washed with water, dried, and placed evenly on 2% agar
559 plates. The agar plate with animals were placed under a camera in the arena of the behavior rig.

560 - **Behavior apparatus**

561 The behavior rig consisted of several apparatuses (see Ohyama et al., 2013 for details and modified
562 by following), including a C-MOS camera (Grasshopper Camera USB3, GS3-U3-41C6M-C,
563 FLIR), infrared 850 nm light-emitting diode (LED) illumination (Waveform Lighting Co.), a 624
564 nm (LED, Waveform Lighting Co.), for optogenetic manipulations, a computer, and a heating
565 panel. Both the camera and LED source were controlled by the computer. LED stimuli were
566 controlled by customized software while larval behaviors were recorded using the Multi-Worm
567 Tracker (MWT) software, a real-time image-analysis software (Swierczek et al., 2011). These two
568 pieces of software were synchronized in the behavior assay to precisely deliver the stimulation
569 during specified time windows.

570 - **Optogenetic stimulation**

571 Before delivering optogenetic stimulation, larvae were placed in the arena for 45 seconds.
572 Subsequently, two 30secons 624 nm LED stimuli were presented successively with a 30-s interval
573 between them. The LED intensity used in each experiment is shown below.

Figure number	**Optogenetic stimulation irradiance (**$\mu W/mm^2$)
Figure 1	0.84
Figure 1 – figure supplement 1	0.84
Figure 1 – figure supplement 2	0.48
Figure 2C-E	5.9
Figure 2F-H	1.8
Figure 2 – figure-supplement 1B-C	5.9
Figure 2 – figure-supplement 1D-E	0.84
Figure 2 – figure-supplement 1H-J	1.8
Figure 5B-D	1.8
Figure 6	1.8
Figure 6 – figure-supplement 1	1.8
Figure 7A-B	0.84
Figure 7 – figure-supplement 1A-D	0.84
Figure 8A-D	3.9
Figure 8E-H	1.8
Figure 8 – figure-supplement 1A-C	1.8

Figure 8 – figure-supplement 1D-E	3.9
Figure 8 – figure-supplement 1F-G	1.8

574 - **Thermal stimulation**

575 To provide heat stimulation, we built thermal control systems with a proportional-integral-
576 derivative (PID) temperature controller (ITC-106VH, Inkbird), a solid-state relay for temperature
577 controllers (SSR-25A, Inkbird), a K-Type thermocouple to detect temperature, and a heat panel.
578 The thermal control system was connected to a custom-built incubator designed to maintain a
579 steady temperature inside the behavior rig at 32°C and warm the agar plates. The temperature of
580 the agar plates was monitored by a thermometer gun (62 MAX+ Compact Infrared Thermometer,
581 Fluke) before and after the experiment to verify the appropriate temperature for *shibire*^{ts1} to be
582 functional. Larvae were sealed in a plastic sieve and pre-heated in a water bath for 10 min to reach
583 32°C before the test. In order to maintain the temperature above 30°C during the test, a replica of
584 the thermal control system mentioned above was installed in the behavior rig, and the behavior rig
585 was pre-heated overnight before any thermal experiment.
586 For *shibire*^{ts1} experiments with heat stimulation, during the first 5 s of the test, larvae were left on
587 the agar plates without LED stimulation. Subsequently, the larvae were optogenetically stimulated
588 with a 624-nm LED for 30 s.

589 **Behavior analysis**

590 Larvae were tracked in real-time using MWT software (https://github.com/Ichoran/choreography).
591 The contour, spine, and center of mass for each larva were generated and recorded by MWT as a
592 function of time. From these tracking data, the key parameters of larval motion were computed
593 using Choreography software (a component of the MWT software package which measured the
594 behavioral parameters offline) as described previously (Ohyama et al., 2013; Ohyama et al., 2015).
595 The behavioral parameters generated by the Choreography algorithm include speed, crabspeed
596 (*i.e.*, speed perpendicular to the body axis), body curvature, angle of head bending, body length,
597 body width, area (dorsal view), and bias (*i.e.,* fractional excess of time spent moving in one
598 direction). In this offline process, objects that were tracked for less than 5 s or moved less than one
599 body length of a larva were rejected. We refer the reader to the open-source package for further
600 details of the software implementations for the above calculations.

601 - **Behavior detection**

602 After extracting behavioral parameters from Choreography, we used an unsupervised machine
603 learning behavior classification algorithm to detect and quantify the following behaviors: hunching

604 (Hunch), head-bending (Turn), stopping (Stop), and peristaltic crawling (Crawl) as previously
605 reported (Masson et al., 2020). Escape rolling (Roll) was detected with a classifier developed using
606 the Janelia Automatic Animal Behavior Annotator (JAABA) platform (Kabra et al., 2013; Ohyama
607 et al., 2015). JAABA transforms the MWT tracking data into a collection of 'per-frame' behavioral
608 parameters and regenerates 2D dorsal-view videos of the tracked larvae. Based on such videos, we
609 defined rolling as a rotation around the body while the larva maintains a C-shape, which results in
610 a movement perpendicular to larval body axis (Supplementary videos 1 and 2). Using this
611 definition, we trained the algorithm in the JAABA platform by labeling ~10,000 randomly chosen
612 frames as rolling or non-rolling to develop the rolling classifier. If a larva did not curl into a C-
613 shape or move sideways, it was labeled as a "non-roller." Every animal with at least one rolling
614 event longer than 0.2 s in a given period was labeled as a "roller" (i.e., it was assumed to have
615 rolled at least 360 degrees), based on the observation that when the start and end of rolling events
616 were precisely measured, the algorithm could identify rolling events completed in 0.2 s.
617 The rejection of false positives, especially at the beginning and the end of each rolling bout,
618 enhanced accuracy. The algorithm integrated these training labels and parameters generated with
619 Choreography in a time series, such as speed, crabspeed, and body curvature, to generate a score
620 for rolling detection. Above a certain threshold, the classifier labeled the frame as rolling. This
621 classifier, which has false negative and false positive rates of 7.4% and 7.8%, respectively (n=102),
622 was utilized to detect rolling in this paper.

623 - **Behavior quantification**

624 The outputs of these behavior detection pipelines served as the input to a customized follow-up
625 MATLAB-based analysis. Only the larvae being tracked fully during the stimulation window were
626 selected for analysis. The percentages of animals performing given behaviors as well as their
627 crawling speed in time series at a frame rate of 10 fps were plotted to depict the behavioral
628 responses. To quantify the behavioral phenotype at the population level, the proportions of larvae
629 that performed given behaviors at least once in the first 5 s after the onset of the stimulation were
630 calculated in percentages. A collection of individual-level parameters (e.g., aggregated durations
631 of rolling throughout the stimulation window, starts and ends of the first rolling event after stimulus
632 onset, starts of the first crawling event after the first rolling event in the stimulation window) were
633 generated and analyzed to describe the effects of stimulation on escape behaviors. Specifically, the
634 starts of the first crawling events after the first rolling events were recorded as 30 s by default if

635 larvae rolled but never initiated crawling during the stimulation window. Furthermore, the
636 cumulative plots of the durations of each rolling event were contrasted to describe the event-level
637 differences.

638 **Larval dissections and immunohistochemistry**

639 Standard immunocytochemical procedures were followed (Patel, 1994). Briefly the CNSs of
640 *Drosophila* larvae were dissected in phosphate-buffered saline (PBS). After dissection, tissues
641 were fixed with 4% paraformaldehyde for 20 min, washed with PBS 3 times and then washed with
642 0.4% Triton X-100 in PBS (PBST) twice. Samples were incubated at room temperature with a
643 blocking solution (5% normal goat serum [NGS]) for 1 h. Next, the samples were incubated with
644 the primary antibody solutions at 4°C overnight and washed for 15 min 6 times. Specially, anti-
645 VGAT was incubated for 48 h to compensate for the permeability, The primary antibodies were
646 diluted at concentrations of 1:3000 for chicken anti-GFP; 1:1000 for rabbit anti-GFP, rabbit anti-
647 GABA and rabbit anti-dsRed; 1:200 for rabbit anti-VGAT; 1:50 for rat anti-Elav, 1:50 for mouse
648 nc82; and 1:20 for rat anti-DN-Cadherin, mouse anti-Fas2, mouse anti-choline acetyltransferase
649 (ChAT), and rabbit anti-VGLUT in 5% NGS. CNS samples were then incubated with a secondary
650 antibody solution at 4°C overnight and washed 15 minutes for 6 times. The secondary antibodies,
651 including anti-chicken Alexa488, anti-rabbit Alexa488, anti-mouse Alexa568, anti-rabbit
652 Alexa568, and anti-rat Alexa568, were all diluted at the concentration of 1:500. These samples
653 were mounted in VECTASHIELD antifade mounting medium and imaged by a Zeiss LSM 710
654 confocal microscope with a 20x/NA0.8 objective lens (Zeiss) and Zen digital imaging software
655 (Zeiss). For quantifying the expression of VGAT or GABA expression, laser power and gains are
656 consistent between samples. All images were processed using Fiji software
657 (https://imagej.new/Fiji, ImageJ, NIH Bethesda).

658 **Immunohistochemistry image analysis**

659 Larval CNS image stacks were processed with FIJI. For figure 5-supplements 1C and D, 4 to 6
660 slices along the z dimension were averaged. The neuropil for VGAT or GABA channels at
661 segments A4 to A6 and cell body regions for elav staining were manually selected as ROIs. The
662 mean intensity of VGAT or GABA was measured and normalized by the mean value of elav
663 staining.

664 **Two-photon calcium imaging assay**

The CNSs of third instar larvae were dissected out in cold Baines external physiological saline (135 mM NaCl, 5 mM KCl, 5 mM TES, 36 mM sucrose, 2 mM $CaCl_2$-$2H_2O$, 4 mM $MgCl_2$.$6H_2O$, pH 7.15), and secured on a poly-L-lysine coated cover glass placed in a small Sylgard plate.

Functional calcium imaging experiments were performed on a customized two-photon microscope equipped with a Galvo-Resonant Scanner (Cambridge) controlled by Scanimage software (mbf BIOSCIENCE) using a 40x/0.80NA water immersion objective (LUMPlanFL, Olympus). A Mai Tai®, Ti:Sapphire Ultrafast Laser (Spectra Physics) tuned to 925 nm was used for excitation of GCaMP protein. Fluorescence signals were collected with photomultiplier tubes (Hamamatsu) after bandpass filtering. Images were acquired by the Galvo-Resonant Scanner for a single plane of the CNS.

Each larva was stimulated by a 620-nm LED (Thorlabs) through the objective three times with a 30-s interval between periods of stimulation. Every stimulus consisted of a 30-ms pulse given every 100 ms for a total of 1 s. Light intensity was measured to be 0.8-1.4 $\mu W/mm^2$. Images were acquired at a resolution of 512 x 512 pixels with a frame rate of 30 fps. Fluorescence intensities were averaged to 6 fps and processed in FIJI, and analyzed in MATLAB with customized scripts. Regions of interest (ROI) were determined by the standard deviation of the full recording. $\Delta F=(F-F_0)/F_0$. F_0 is the average of images taken 10 frames (i.e., 1.7 s) before stimulation. F is the mean value of the fluorescence in the ROI averaged every 5 frames from the start of the 5-s period before stimulation to end of the 15-s period after the onset of each stimulation. For each larva, ΔF is obtained through averaging the ΔF during the three stimulation periods. The peak ΔFs were the maximal values selected from the onset of stimulation to 15 s after stimulus onset.

Statistics

The probabilities for each response were analyzed by Chi-square tests. For the other parameters, when multiple groups were tested, their normality was examined first. If the normality assumption was rejected, Kruskal-Wallis tests were performed for multiple group variance comparisons, followed by multiple-comparison-corrected Wilcoxon–Mann–Whitney U tests as post hoc pairwise comparisons. If normality was met, analysis of variance (ANOVA) was performed for variance comparisons and multiple-comparison-corrected student's t-tests were utilized for pairwise comparisons. For two group comparisons, the Wilcoxon–Mann–Whitney U test was conducted if the normality assumption was offended, and the student's t-test was applied if normality was met. All analyses were conducted with MATLAB.

Data availability statement

The original contributions presented in this study are included in the article/supplemental material; further inquiries may be directed to the corresponding author.

Conflict of interests

The authors declare that the research was conducted in the absence of any commercial or financial relationships that could be construed as a potential conflict of interests.

Author contributions

Conceptualization, J.Z. and T.O. Writing – Original Draft, J.Z. and T.O; Writing – Review & Editing, J.Z., J-C.B., and T.O. Formal Analysis, J.Z., J-C.B., and T.O. Performing experiments, J.Z., J-C.B., J.N., Y.Q.Z., and T.O. Supervision, T.O.

Funding

This work was funded by McGill University, the National Sciences and Engineering Research Council (NSERC, RGPIN/04781-2017), the Canadian Institute of Health Research (CIHR, PTJ-376836), the Fonds de recherche du Quebéc – Nature et technologies (FRQNT, 2019-N-25523), and the Canada Foundation for Innovation (CFI, CFI365333). J-C.B was supported by Fonds de recherche du Quebéc-Santé (FRQS) graduate training award.

Acknowledgements

We thank J.W. Truman, A. Cardona, and M. Zlatic for generating and sharing the split Gal4 lines. J. Truman and M. Zlatic for constructive inputs on the project. Confocal images were collected at the McGill University Advanced Bio Imaging Facility (ABIF), RRID:SCR_017697. We also thank the Bloomington stock center for providing fly stocks. We thank members of Ohyama lab for critical comments on the manuscript.

Inclusion and diversity

One or more of authors of this paper self-identifies as a member of the LGBTYQ+ community.

727 **Figure legends:**

728 **Figure 1. Activation of SS04185 inhibits rolling evoked by activation of Basin neurons**

729 (A) Schematic of *Drosophila* larval escape behavior sequence.

730 (B) Ethograms of Basin activation (top panel) and co-activation of SS04185 and Basins (bottom
731 panel). Each row represents an individual larva. Pink, blue, green, orange, and purple lines
732 represent bouts of rolling, turning, crawling, backward crawling, and hunching. The red bar and
733 dashed lines indicate the time window during which neural activation was present. Genotypes:
734 *20xUAS-IVS-CsChrimson::mVenus/+;+; R72F11-Gal4/+* (top); *20xUAS-IVS-*
735 *CsChrimson::mVenus/+; R54B01-Gal4.AD/+; R46E07-Gal4.DBD/ R72F11-Gal4* (bottom).
736 Genotypes in (C-D, F-I) are the same as those mentioned here.

737 (C) Time series of larval crawling speed during co-activation of SS04185 and Basins (red) and
738 activation of Basins alone (black). Shaded areas represent the standard error. The red bar and
739 dashed lines denote the optogenetic stimulation window.

740 (D) Time series of rolling probabilities of larvae during co-activation of SS04185 and Basins (red)
741 and activation of Basins alone (black). Shaded areas represent 95% confidential intervals for
742 rolling probabilities. The red bar and dashed lines denote the optogenetic stimulation window.

743 (E) Rolling probabilities of larvae with activation of different neurons. Error bars represent the
744 95% confidence interval. Genotypes from left to right: 1) *20xUAS-IVS-CsChrimson::mVenus/+; ; ,*
745 2) *20xUAS-IVS-CsChrimson::mVenus/+; R54B01-Gal4.AD/+; R46E07-Gal4.DBD/+*, 3)
746 *20xUAS-IVS-CsChrimson::mVenus/+; ; R72F11-Gal4/+*, 4) *20xUAS-IVS-*
747 *CsChrimson::mVenus/+; R54B01-Gal4.AD/+; R46E07-Gal4.DBD/ R72F11-Gal4.* n = 120, 118,
748 231, 155 from left to right. Statistics: Chi-square test, $\chi^2 = 0$, $p > 0.05$ for the first two groups; χ^2
749 $= 83.85$, $p < 0.001$ for the last two groups; and $\chi^2 = 365.51$, $p < 0.001$ for the comparison between
750 the first two groups and the last two groups.

751 (F) Cumulative plot of rolling duration. Statistics: Mann-Whitney U test, $p < 0.001$, n = 652, 120.

752 (G) A violin plot showing start of first rolling bout for each larva during stimulation. Statistics:
753 Mann-Whitney U test, $p = 0.027$, n = 225, 89.

754 (H) A violin plot displaying end of first rolling bout for each larva during stimulation. Statistics:
755 Mann-Whitney U test, $p < 0.001$, n = 225, 89.

756 (I) A violin plot presenting start of first crawling bout for each larva during stimulation. Statistics:
757 Mann-Whitney U test, $p < 0.001$, n = 214, 70.

758 $^{**}p < 0.01$, $^{***}p < 0.001$.

759

760 **Figure 1 - Figure supplement 1. Activation of SS04185 inhibits rolling**

761 (A) Crawling probabilities of larvae with the activation of SS04185-expressing neurons. Error bars,
762 95% confidence interval. Genotypes: *20xUAS-IVS-CsChrimson::mVenus/+;;* (black); *20xUAS-*
763 *IVS-CsChrimson::mVenus/+; R54B01-Gal4.AD/+; R46E07-Gal4.DBD/+* (red). Genotypes in (B-
764 D) are the same as shown here. n = 308, 172. Statistics: Chi-square test, $\chi^2 = 2.32$, $p > 0.05$.

765 (B) Turning probabilities of larvae with activation of SS04185-expressing neurons. Error bars,
766 95% confidence interval. n = 308, 172. Statistics: Chi-square test, $\chi^2 = 1.77$, $p > 0.05$.

767 (C) Hunching probabilities of larvae with activation of SS04185-expressing neurons. Error bars,
768 95% confidence interval. n = 308, 172. Statistics: Chi-square test, $\chi^2 = 0.35$, $p > 0.05$.

769 (D) Stopping probabilities of larvae with activation of SS04185-expressing neurons. Error bars,
770 95% confidence interval. n = 308, 172. Statistics: Chi-square test, $\chi^2 = 3.97$, $p = 0.046$.

771 (E) A violin plot of total time spent rolling for each individual larva during stimulation. Statistics:
772 Mann-Whitney U test, $p < 0.001$, n = 225, 89.

773 (F) Time series of crawling probabilities of SS04185 and Basin coactivation larvae (green) and
774 Basin activation only larvae (black). Shaded areas show 95% confidential intervals of the crawling
775 probabilities. Dashed lines display the window of optogenetic stimulation. Genotypes: *20xUAS-*
776 *IVS-CsChrimson::mVenus/+; +; R72F11-Gal4/+* (control); *20xUAS-IVS-*
777 *CsChrimson::mVenus/+; R54B01-Gal4.AD/+; R46E07-Gal4.DBD/R72F11-Gal4* (SS04185).
778 Genotypes in (G-H) are the same as mentioned here. n = 228, 124.

779 (G) A violin plot of interval between first roll and next crawl. Statistics: Mann-Whitney U test, p
780 > 0.05, n = 151, 74.

781 (H) Crawling probabilities of SS04185 and Basin coactivation larvae (red) and Basin activation
782 only larvae (black). Error bars, 95% confidence interval. n = 228, 124. Statistics: Chi-square test,
783 $\chi^2 = 28.36$, $p < 0.001$.

784 (I) A violin plot of crawling speed ratio of larvae with null, SS04185 neuron, Basin, SS04185
785 neuron and Basin activation (from left to right). Crawling speed ratio = crawling speed 5 to 10 s
786 after stimulation onset / crawling speed 0 to 5 s before stimulation onset. Statistics: Kruskal-Wallis
787 test: H = 144, $p < 0.001$; Bonferroni corrected Mann-Whitney U test: $p > 0.05$ for two groups on
788 the left and two groups on the right. n = 308, 172, 227, 124. Genotypes from left to right: 1)

789 *20xUAS-IVS-CsChrimson::mVenus/+;;* ; 2) *20xUAS-IVS-CsChrimson::mVenus/+; R54B01-*
790 *Gal4.AD/+; R46E07-Gal4.DBD/+*; 3) *20xUAS-IVS-CsChrimson::mVenus/+;; R72F11-Gal4/+*;
791 4) *20xUAS-IVS-CsChrimson::mVenus/+; R54B01-Gal4.AD/+; R46E07-Gal4.DBD/R72F11-Gal4.*
792 $^{**}p < 0.01$, $^{***}p < 0.001$.
793
794 **Figure 1 - Figure supplement 2. Activation of SS04185 inhibits rolling**
795 (A) Time series of rolling probabilities of larvae during co-activation of SS04185 and Basins (red)
796 and activation of Basins alone (black). Shaded areas represent 95% confidential intervals for
797 rolling probabilities. The red bar and vertical dashed lines denote the optogenetic stimulation
798 window. Genotypes: 1) *20xUAS-IVS-CsChrimson::mVenus/+; ; R72F11-Gal4/+* (control), 2)
799 *20xUAS-IVS-CsChrimson::mVenus/+; R54B01-Gal4.AD/+; R72F11-Gal4/+* (54B01-AD), 3)
800 *20xUAS-IVS-CsChrimson::mVenus/+; ; R72F11-Gal4/ R46E07-Gal4.DBD* (46E07-DBD), 4)
801 *20xUAS-IVS-CsChrimson::mVenus/+; R54B01-Gal4.AD/+; R46E07-Gal4.DBD/ R72F11-Gal4*
802 (SS04185). Genotypes in (B)-(C) are the same as mentioned here. n = 162, 209, 103, 153.
803 (B) Rolling probabilities of larvae plotted in (A) in the first 5s of stimulation. Error bars represent
804 the 95% confidence interval. n = 162, 209, 103, 153 from left to right. Statistics: Chi-square test,
805 $\chi^2 = 6.66$, $p > 0.05$ for the left three groups and $\chi^2 = 72.52$, $p < 0.001$ for the comparison between
806 the left three groups and the SS04185 group.
807 (C) A violin plot of total time spent rolling for each individual larva during stimulation. Statistics:
808 Kruskal-Wallis test: H = 105.99, $p < 0.001$; Bonferroni-corrected Mann-Whitney U test, $p > 0.05$
809 for the comparison between control and 54B01-AD; $p < 0.001$ for all other pair-wise comparisons,
810 n = 151, 172, 100, 86.
811 $^{**}p < 0.01$, $^{***}p < 0.001$.
812
813 **Figure 2. SS04185-DN, but not SS04185-MB, inhibits rolling when co-activated with Basins**
814 (A) Morphology of SS04185 neurons. GFP, grey (left), green (right); nc82, magenta. Anterior, up;
815 dorsal view; scale bar, 100 µm. Genotype: *10xUAS-IVS-myr::GFP/+; R54B01-Gal4.AD/+;*
816 *R46E07-Gal4.DBD/+*.
817 (B) Kenyon cells are less labeled in SS04185 with MB>Killer Zipper. CsChrimson::mVenus
818 expression in Kenyon cells of SS04185 in Control and SS04185 with Killer Zipper in mushroom
819 body (MB). mVenus, grey (left), green (right); nc82, magenta. Anterior, up; dorsal view; scale bar,

820 20 μm. Genotype: *20xUAS-IVS-CsChrimson::mVenus/+; R54B01-Gal4.AD/+; R46E07-*
821 *Gal4.DBD/+* (control); *20xUAS-IVS-CsChrimson::mVenus/+; R13F02-LexA,LexAop-*
822 *KZip*$^+$*/R54B01-Gal4.AD; R72F11-Gal4/R46E07-Gal4.DBD* (MB>KZip$^+$).
823 (C) Rolling probabilities of larvae with activation of SS04185 reduce the expression of
824 CsChrimson in mushroom body (MB) neurons. Error bars, 95% confidence interval. n = 78, 55,
825 100 from left to right. Statistics: Chi-square test, $\chi^2 = 2.32$, $p > 0.05$ for the two groups with
826 SS04185 expression; $\chi^2 = 37.50$, $p < 0.001$ for the comparison between the two groups on the left;
827 $\chi^2 = 70.45$, $p < 0.001$ for the comparison between the groups with *MB>KZip*$^+$ expression which
828 reduce expression of CsChrimson in MB. Genotypes: *20xUAS-IVS-CsChrimson::mVenus/+;*
829 *R13F02-LexA,LexAop-KZip*$^+$*/+; R72F11-Gal4/+* (black); *20xUAS-IVS-*
830 *CsChrimson::mVenusR54B01-Gal4.AD/+; R46E07-Gal4.DBD/R72F11-Gal4* (orange); *20xUAS-*
831 *IVS-CsChrimson::mVenus/+; R13F02-LexA,LexAop-KZip*$^+$*/R54B01-Gal4.AD; R72F11-*
832 *Gal4/R46E07-Gal4.DBD* (red). Genotypes in (D-E) are the same as mentioned here.
833 (D) Cumulative plot of rolling duration. Statistics: Kruskal-Wallis test: H = 8.28, $p = 0.016$;
834 Bonferroni-corrected Mann-Whitney U test, $p > 0.05$ for all pairwise post-hoc tests, n = 103, 20,
835 27 from left to right.
836 (E) A violin plot of start of first crawling bout for each larva during stimulation. Statistics: Kruskal-
837 Wallis test: H = 15.02, $p < 0.001$; Bonferroni-corrected Mann-Whitney U test, $p > 0.05$ for the two
838 groups with SS04185 expression; $p < 0.001$ for the comparison between the group without
839 SS04185 expression and the groups with full SS04185 expression, n = 65, 20, 7 from left to right.
840 (F) The probabilities of larval rolling during first 5 s of stimulation. Error bars, 95% confidence
841 interval. n = 101, 126. Statistics: Chi-square test, $\chi^2 = 4.27$, $p = 0.039$. Genotype: *13xLexAop2-*
842 *IVS-CsChrimson::tdTomato/w*$^+$*, hs-FLP; R54B01-Gal4.AD/72F11-LexA; 20XUAS-(FRT.stop)-*
843 *CsChrimson::mVenus/R46E07-Gal4.DBD.* Genotypes in (G-H) are the same as mentioned here.
844 (G) Cumulative plot of rolling duration. Statistics: Mann-Whitney U test, $p < 0.001$, n = 350, 473.
845 (H) A violin plot of start of first crawling bout for each larva during stimulation. Statistics: Mann-
846 Whitney U test, $p < 0.001$, n = 97, 120.
847 $^{**}p < 0.01$, $^{***}p < 0.001$.
848
849 **Figure 2 - Figure supplement 1. SS04185-DN inhibits rolling**

850 (A) Morphology of SS04185 neurons with split Gal4 inhibition in mushroom body (MB). GFP,
851 Green. Anterior, up; dorsal view; scale bar, 100 μm. Genotype: *20xUAS-IVS-*
852 *CsChrimson::mVenus/+; R13F02-LexA,LexAop-KZip*$^{+}$*/R54B01-Gal4.AD; R72F11-*
853 *Gal4/R46E07-Gal4.DBD.*
854 (B) Time series of rolling probabilities of larvae with split Gal4 inhibition in MB (black), SS04185
855 activation (orange), and both SS04185 activation and split Gal4 inhibition in MB (red). Shaded
856 areas show 95% confidential intervals of rolling probabilities. The red bar and dashed lines display
857 the window of optogenetic stimulation. Genotypes: *20xUAS-IVS-CsChrimson::mVenus/+;*
858 *R13F02-LexA,LexAop-KZip*$^{+}$*/+; R72F11-Gal4/+* (black); *20xUAS-IVS-CsChrimson::mVenus/+;*
859 *R54B01-Gal4.AD/+; R46E07-Gal4.DBD/R72F11-Gal4* (orange); *20xUAS-IVS-*
860 *CsChrimson::mVenus/+; R13F02-LexA,LexAop-KZip*$^{+}$*/R54B01-Gal4.AD; R72F11-*
861 *Gal4/R46E07-Gal4.DBD* (red). Genotypes in (C) are the same as mentioned here.
862 (C) A violin plot of total time spent rolling for each individual larva during stimulation. Statistics:
863 Kruskal-Wallis test: H = 21.05, $p < 0.001$; Bonferroni-corrected Mann-Whitney U test, $p > 0.05$
864 for the two groups with SS04185 expression; $p < 0.001$ for the comparison between the group
865 without SS04185 expression and the two groups with SS04185 expression, n = 66, 17, 21 from
866 left to right.
867 (D) Time series of rolling probabilities of larvae with Basin activation (black), or Basin and MB
868 coactivation (red). The red bar and dashed lines display the window of optogenetic stimulation
869 eliciting larval escape responses. Shaded areas show 95% confidential intervals of rolling
870 probabilities. n = 150, 143. Genotype: *20xUAS-IVS-CsChrimson::mVenus/+; +; R72F11-Gal4/+*
871 (control); *20xUAS-IVS-CsChrimson::mVenus/+;+; MB247-Gal4/R72F11-Gal4* (MB247).
872 Genotypes in (E) are the same as mentioned here.
873 (E) Binned larval rolling probabilities during the first 5 s of stimulation in (D). Error bars, 95%
874 confidence interval. n = 150, 143. Statistics: Chi-square test, $\chi^2 = 3.80$, $p > 0.05$.
875 (F) and (G) show immunostaining of SS04185-expressing neurons. SS04185, Green. Anterior, up;
876 dorsal view; scale bar, 100 μm Genotype: *w+, hs(KDRT.stop)FLP/13xLexAop2-IVS-*
877 *CsChrimson::tdTomato; R54B01-Gal4.AD/72F11-LexA; 20xUAS-FRT(stop)-*
878 *CsChrimson::mVenus/R46E07-Gal4.DB.* Genotypes in (H-K) are the same as mentioned here. (F)
879 has both SS04185-DN and SS04185-MB expression only, and (G) has SS04185-MB expression.

880 (H) Time series of rolling probabilities of larvae with SS04185-MB activation (black), or
881 SS04185-MB and SS04185-DN coactivation (red). The red bar and dashed lines display the
882 window of optogenetic stimulation eliciting larval escape responses. Shaded areas show 95%
883 confidential intervals of rolling probabilities.
884 (I) A violin plot of total time spent rolling for each individual larva during stimulation. Statistics:
885 Mann-Whitney U test, $p < 0.001$, n = 99, 124.
886 (J) A violin plot of end of first rolling bout for each larva during stimulation. Statistics: Mann-
887 Whitney U test, $p < 0.001$, n = 99, 124.
888 (K) Time series of turning probabilities of larvae with SS04185-MB activation (black), or
889 SS04185-MB and SS04185-DN coactivation (red). The red bar and dashed lines display the
890 window of optogenetic stimulation eliciting larval escape responses. Shaded areas show 95%
891 confidential intervals of turning probabilities.
892 $^{**}p < 0.01$, $^{***}p < 0.001$.
893
894 **Figure 3. SS04185-DN is identical to SeIN128**
895 (A) TEM neuron reconstruction of SeIN128 neurons. Left panel: anterior, up; dorsal view. Right
896 panel: anterior, up; dorsal, right; lateral view. Red dots, presynaptic sites. Cyan dots, postsynaptic
897 sites.
898 (B) A transverse section of larval CNS from EM reconstruction data. SeIN128 (green), Basins
899 (blue), and A00c (orange) are located in ventromedial tract (VM). mdIV, red; magenta, neural
900 tracts. DM, dorsomedial tract; VM, ventromedial tract. Dorsal, up; anterior view; scale bar, 1 µm.
901 (C) Cartoon generated based on transverse section of SeIN128, Basin-1 to Basin-4, A00c, and
902 mdIV from EM neuron reconstruction data and (D). Nerve tracts are shown in magenta. Dorsal,
903 up; posterior view. DM, dorsomedial tract; VM, ventromedial tract; CI, central-intermediate tract;
904 CL, central-lateral tract; DL, dorsolateral tract; VL, ventrolateral tract. SeIN128, green; Basin-1 to
905 Basin-4, blue; A00c, orange; mdIV, red.
906 (D) SS04185-expressing neurons co-stained with N-Cadherin. A cell body of SS04185-
907 Descending neuron located in ventral part of the subesophageal zone (SEZ). SS04185, Green; N-
908 Cadherin, magenta. Anterior, up; left, dorsal view; right, longitudinal section; scale bar, 100 µm.
909 Genotype: *10xUAS-IVS-myr::GFP/+; R54B01-Gal4.AD/+; R46E07-Gal4.DBD/+*. SS04185,
910 Green; Cadherin, magenta. Anterior, left, dorsal, up; lateral view; scale bar, 100 µm.

911 (E) Transverse section of SS04185-DN co-stained with Fas2. SS04185-DN located at
912 ventromedial tract (VM). SS04185, Green; Fas2, magenta. Dorsal, up; posterior view; scale bar,
913 20 µm. DM, dorsomedial tract; VM, ventromedial tract; CI, central-intermediate tract; CL, central-
914 lateral tract; DL, dorsolateral tract; VL, ventrolateral tract. Genotype: *10xUAS-IVS-myr::GFP/+;*
915 *R54B01-Gal4.AD/+; R46E07-Gal4.DBD/+.*
916 (F, H, J) SS04185-DN co-localized with Basins or A00C neuron tract but not MdIV. SS04185,
917 Green; Basins (F), A00c (H) or mdIV (J), magenta;. Genotype: *w; R54B01-Gal4.AD/R72F11-*
918 *LexA(F) 71A10-LexA(H) or ppk1.9-LexA(J); R46E07-Gal4.DBD/13xLexAop2-IVS-*
919 *CsChrimson::tdTomato,20xUAS-IVS-GCaMP6s.* Top panel: anterior, up; dorsal view; scale bar,
920 10 µm. Bottom panel: dorsal, up; posterior view; scale bar, 5 µm.
921 (G, I, K) SeIN128, Basin-2, A00c or mdIV morphologies from the TEM neural reconstruction.
922 Anterior, up; dorsal view. SS04185, green; Basin-2, blue; A00C, orange; mdIV, red.
923
924 **Figure 4. SeIN128 receives input from Basin and A00c neurons**
925 (A) Summary of the connectivity between SeIN128 and the escape circuit. SeIN128 receives
926 inputs from Basin-2 and A00c and provide feedback to Basin-2 and A00c. Synapse number shown
927 next to connection arrows, where line width is proportional to synapse number. All connections in
928 the ventral nerve cord are shown except unilateral synapses, <5 synapses, between neurons. Each
929 polygon represents a pair of the indicated neuron and segment (segment number is shown under
930 the neuron name). SeIN128, green; Basin-2, blue; A00c, orange; mdIV, red.
931 (B, C) SeIN128 is functionally downstream of Basins (B) or A00c (C). Calcium transients, $\Delta F/F_0$
932 traces of GCaMP6s in SeIN128 axons (black line, mean; gray line, single larva) during 610-nm
933 optogenetic activation of Basins at various intensities. Vertical gray line represents optogenetic
934 activation. Genotype: *w; R72F11-LexA (B) or R71A10-LexA (C) /R54B01-Gal4.AD; 13xLexAop2-*
935 *IVS—CsChrimson::tdTomato, 20xUAS-IVS-GCaMP6s/R46E07-Gal4.DBD.*
936 (D) A00c responses are faster and stronger than SeIN128 responses during activation of Basins.
937 Calcium transients (black line, mean; gray line, single larva) represented by $\Delta F/F_0$ in A00c by of
938 610-nm optogenetic activation of Basins at various intensities. Genotype: *w; R72F11-LexA/+;*
939 *13xLexAop2-IVS-CsChrimson::tdTomato, 20xUAS-IVS-GCaMP6s/R71A10-Gal4.*

940 For (B) to (D), irradiances from left to right are 0.04, 0.1, 0.3, 0.5, and 1.4 μW/mm^2. For each
941 irradiance (n = 6), individual traces are shown with gray lines whereas the average of individuals
942 is shown in black. The shaded gray area indicates the period of optogenetic activation (0 to 1 s).
943 (E) The timing of the peak $\Delta F/F_0$ correlated with the identity of the neurons but not the peak $\Delta F/F_0$
944 value. SeIN128 neurons are shown as orange dots, whereas A00c is shown as a green dot.
945
946 **Figure 4 - Figure supplement 1. SeIN128 is downstream of Basin and A00c neurons**
947 (A) Connectivity among Basin, A00c, and SeIN128. Each line represents synaptic connections
948 from the pre-synaptic neurons (left) to the post-synaptic neurons (right). Line widths are
949 proportional to the counts of the synapses.
950 (B) SeIN128 does not respond to light stimulation when all-trans retinal is not fed. Calcium
951 transients, $\Delta F/F_0$ traces of GCaMP6s in SeIN128 axons (black line, mean; gray line, single larva)
952 during 610-nm optogenetic activation of Basins at various intensities. Vertical gray line represents
953 optogenetic activation. The shaded gray area indicates the period of optogenetic activation (0 to 1
954 s). Irradiance, 1.4 μW/mm^2. n=4. Genotype: *w; R72F11-LexA (left panel) or R71A10-LexA (right*
955 *panel) /R54B01-Gal4.AD; 13xLexAop2-IVS-CsChrimson::tdTomato, 20xUAS-IVS-*
956 *GCaMP6s/R46E07-Gal4.DBD.*
957 (C) Peak $\Delta F/F_0$ increased with increasing irradiance in both SeIN128 and A00c neurons. The
958 orange line corresponds with Figure 4B; yellow line corresponds with Figure 4C; and green line
959 corresponds with Figure 4D.
960
961 **Figure 4 - Figure supplement 2. Synapses from SeIN128 to Basin-2 are located near Basin-2**
962 **outputs**
963 (A) Basin-2 morphology and cell body location reported in EM reconstruction dataset (A1, left
964 hemi-segment). Dorsal view. Red lines, presynaptic sites; cyan lines, postsynaptic sites.
965 (B) A zoomed-in view of the square in (A).
966 (C) SeIN128 morphology and cell body location reported in EM reconstruction dataset (right).
967 Dorsal view. Red lines, presynaptic sites; cyan lines, postsynaptic sites.
968 (D) A zoomed-in view of the square in (C).
969 (E) Connections between SeIN128 and Basin-2. Dorsal view. Red lines, presynaptic sites of
970 SeIN128; cyan lines, postsynaptic sites of Basin-2; brown lines, presynaptic sites of Basin-2.

971 (F) Zoomed-in views of squares in (E).
972 (G) EM view of left top panel in (F). Green, SeIN128. Blue, Basin-2. White arrows show SeIN128
973 presynaptic sites adjacent to Basin-2. Yellow arrows are two presynaptic sites of Basin-2.
974
975 **Figure 5. SeIN128 is GABAergic and negatively controls rolling**
976 (A) Immunostaining of SeIN128 cell body (green) and GABAergic neuron (magenta). Genotype:
977 *10xUAS-IVS-myr::GFP; R54B01-Gal4.AD/13xLexAop-dsRed; R46E07-Gal4.DBD/Trojan-GAD-*
978 *T2A-LexA.* White triangles indicate locations of SeIN128 cell bodies. Anterior, up; dorsal view;
979 scale bar, 10 μm.
980 (B) Time series of rolling probabilities of larvae with Basin activation (black), or VGAT RNAi in
981 SS04185 and Basin activation (red). The red bar and dashed lines display the window of
982 optogenetic stimulation eliciting larval escape responses. Shaded areas show 95% confidential
983 intervals of rolling probabilities. Genotypes: *13xLexAop2-IVS-CsChrimson::mVenus; R72F11-*
984 *LexA/+; HMS02355/+* (black); *13xLexAop2-IVS-CsChrimson::mVenus; R72F11-LexA/R54B01-*
985 *Gal4.AD; HMS02355/R46E07-Gal4.DBD* (red). Genotypes in (C, D) are the same as mentioned
986 here.
987 (C) Binned larval rolling probabilities during first 5 s of stimulation in (A). Error bars, 95%
988 confidence interval. n = 110, 73. Statistics: Chi-square test, $\chi^2 = 9.34$, $p < 0.001$.
989 (D) Cumulative plot of rolling duration. Statistics: Mann-Whitney U test, $p = 0.015$, n = 55, 73.
990 $^{**}p < 0.01$, $^{***}p < 0.001$.
991
992 **Figure 5 - Figure supplement 1. SeIN128 is GABAergic**
993 (A) Immunostaining of SeIN128 cell body (green) and glutamatergic neuron (magenta). Genotype:
994 *10xUAS-IVS-myr::GFP/+; R54B01-Gal4.AD/+; R46E07-Gal4.DBD/+.*
995 (B) Immunostaining of SeIN128 cell body (green) and cholinergic neuron (magenta). Genotype:
996 *10xUAS- IVS-myr::GFP/+; R54B01-Gal4.AD/+; R46E07-Gal4.DBD/+.*
997 In (A)-(B), white triangles indicate locations of SeIN128 cell bodies. Anterior, up; dorsal view;
998 scale bar, 10 μm.
999 (C) Normalized anti-GABA fluorescence intensities in the neuropil by anti-Elav staining in
1000 segments A4 to A6. A.U., arbitrary unit. Genotype: *w; ; R57C10-Gal4 /+* (black) and *w; ; R57C10-*
1001 *Gal4 /UAS-HMS02355* (red). Statistics: Student's t test, ** $p = 0.0106$, n = 7.

1002 (D) Normalized anti-VGAT fluorescence intensities in the neuropil by anti-Elav staining in
1003 segments A4 to A6. A.U., arbitrary unit. Genotype: *w; ; R57C10-Gal4 /+* (black) and *w; ; R57C10-*
1004 *Gal4 /UAS-HMS02355* (red). Statistics: Student's t test, p = 0.0031, n = 6. * p = 0.0295.
1005
1006 **Figure 6. Inhibition of SeIN128 prolongs rolling and delays initiation of crawling**
1007 (A) Time series of rolling probabilities of larvae with Basin activation (black), or SS04185
1008 inhibition and Basin activation (red). Shaded regions show 95% confidential intervals of rolling
1009 probabilities. Genotypes: *13xLexAop2-IVS-CsChrimson::mVenus; R72F11-LexA/+; UAS-*
1010 *TeTxLC.tnt/+* (black); *13xLexAop2-IVS-CsChrimson::mVenus; R72F11-LexA/R54B01-Gal4.AD;*
1011 *UAS-TeTxLC.tnt/R46E07-Gal4.DBD* (red). Genotypes in (B-F) are the same as mentioned here.
1012 (B) Rolling probabilities during first 5 s of stimulation in (A). Error bars, 95% confidence interval.
1013 n = 241, 164. Statistics: Chi-square test, χ^2 = 44.02, p < 0.001.
1014 (C) A violin plot of total time spent rolling for each individual larva during stimulation. Statistics:
1015 Mann-Whitney U test, p < 0.001, n = 221, 258.
1016 (D) Cumulative plot of rolling duration. Statistics: Mann-Whitney U test, p < 0.001, n = 160, 154.
1017 (E) A violin plot of end of first rolling bout for each larva during stimulation. Statistics: Mann-
1018 Whitney U test, p < 0.001, n = 160, 154.
1019 (F) A violin plot of start of first crawling bout for each larva during stimulation. Statistics: Mann-
1020 Whitney U test, p < 0.001, n = 65, 105.
1021 **p < 0.01, ***p < 0.001.
1022
1023 **Figure 6 - Figure supplement 1. SeIN128 inhibition enhances rolling**
1024 (A) Time series of rolling probabilities of larvae with Basin activation (black), or SS04185
1025 inhibition and Basin activation (red). Larvae were incubated with heat to trigger the effect of
1026 shibire^{ts1}. The red bar and dashed lines display the window of optogenetic stimulation eliciting
1027 larval escape responses. Shaded areas show 95% confidential intervals of rolling probabilities.
1028 Genotypes: *13xLexAop2-IVS-CsChrimson::mVenus;R72F11-LexA/+; 20xUAS-TTS-Shibire/+*
1029 (black); *13xLexAop2-IVS-CsChrimson::mVenus; R72F11-LexA/R54B01-Gal4.AD; 20xUAS-TTS-*
1030 *Shibire/R46E07-Gal4.DBD* (red). Genotypes in (B-G) are the same as mentioned here.
1031 (B) Binned larval rolling probabilities during first 5 s of stimulation in (A). Error bars, 95%
1032 confidence interval. n = 134, 143. Statistics: Chi-square test, χ^2 = 12.33, p < 0.001.

1033 (C) A violin plot of total time spent rolling for each individual larva during stimulation. Statistics:
1034 Mann-Whitney U test, $p > 0.05$, n = 85, 115.
1035 (D) Cumulative plot of rolling duration. Statistics: Mann-Whitney U test, $p > 0.05$, n = 219, 352.
1036 (E) A violin plot of start of first rolling bout for each larva during stimulation. Statistics: Mann-
1037 Whitney U test, $p > 0.05$, n = 85, 115.
1038 (F) A violin plot of end of first rolling bout for each larva during stimulation. Statistics: Mann-
1039 Whitney U test, $p = 0.013$, n = 85, 115.
1040 (G) A violin plot of start of first crawling bout for each larva during stimulation. Statistics: Mann-
1041 Whitney U test, $p = 0.034$, n = 32, 22.
1042 $^{**}p < 0.01$, $^{***}p < 0.001$.
1043
1044 **Figure 7. SeIN128 sends feedback inhibition to Basins**
1045 (A) Rolling probabilities for larvae with GABAR-RNAi in their Basin neurons. From left to right,
1046 the genotypes are *20xUAS-IVS-CsChrimson::mVenus/+; ; R72F11-Gal4/+* (black*), 20xUAS—IVS-*
1047 *CsChrimson::mVenus/+; ; R72F11-Gal4/UAS-HMC03388* (blue), *20xUAS-IVS-*
1048 *CsChrimson::mVenus/+; ; R72F11-Gal4/UAS-JF02989* (green), *20xUAS-IVS-*
1049 *CsChrimson::mVenus/+; ; R72F11-Gal4/UAS-HMC02975* (yellow), and 20x*UAS-IVS-*
1050 *CsChrimson::mVenus/+; ; R72F11-Gal4/UAS-HMC03643* (orange). Genotypes in (B) are the
1051 same as mentioned here. N = 320, 205, 159, 183, 182 from left to right. Statistics: Chi-square test,
1052 Bonferroni correction. GABA-B-R1[1] group: $\chi^2 = 8.76$, $p = 0.012$. GABA-B-R1[2] group: $\chi^2 = 24.70$,
1053 $p < 0.001$. GABA-B-R2 group: $\chi^2 = 25.77$, $p < 0.001$. GABA-A-R group: $\chi^2 = 16.29$, $p < 0.001$.
1054 (B) Cumulative plot of rolling duration. Statistics: Kruskal-Wallis test: H = 69.52, $p < 0.001$;
1055 Bonferroni-corrected Mann-Whitney U test, $p < 0.001$ between control and the GABA-B-R11,
1056 GABA-B-R12, and GABA-B-R2 RNAi groups; $p < 0.001$ between GABA-A-R and all other
1057 RNAi groups. Sample sizes for the colored bars from top (control, black) to bottom (GABA-A-R,
1058 red); n = 520, 488, 387, 582, 306.
1059 (C) Summary of peak $\Delta F/F_0$ in Basin axons with or without SeIN128 activation under various
1060 irradiances. Control groups shown in black are without SeIN128 activation while experimental
1061 groups shown in red are with SeIN128 activation. Statistics: Mann-Whitney U test, $p > 0.05$ for
1062 irradiances of 0.04, 0.1, 1.4 μW/mm^2; $p = 0.016$ for irradiance of 0.3 μW/mm^2; $p = 0.032$ for
1063 irradiance of 0.5 μW/mm^2. Genotype: *20xUAS-Syn21-opGCaMP6s, 10xUAS-Syn21-*

1064 *CsChrimson88::tdTomato/+; CyO/+;R72F11-Gal4/TM6* (black); *20xUAS-Syn21-*
1065 *opGCaMP6s,10xUAS-Syn21-CsChrimson88::tdTomato/+;CyO/R54B01-Gal4.AD;R72F11-*
1066 *Gal4/R46E07-Gal4.DBD* (red).
1067 $^{**}p < 0.01$, $^{***}p < 0.001$.
1068
1069 **Figure 7 - Figure supplement 1. SeIN128 sends feedback inhibition to Basins**
1070 (A) A violin plot of total time spent rolling for each individual larva with GABAR-RNAi in their
1071 Basin neurons during stimulation. Statistics: Kruskal-Wallis test: H = 110.86, $p < 0.001$;
1072 Bonferroni-corrected Mann-Whitney U test, $p < 0.001$ for all RNAi groups, n = 271, 194, 154,
1073 178, 174 from left to right. The genotypes are *20xUAS-IVS-CsChrimson::mVenus/+; ; R72F11-*
1074 *Gal4/+* (black*), 20xUAS—IVS-CsChrimson::mVenus/+; ; R72F11-Gal4/UAS-HMC03388* (blue),
1075 *20xUAS-IVS-CsChrimson::mVenus/+; ; R72F11-Gal4/UAS-JF02989* (green), *20xUAS-IVS-*
1076 *CsChrimson::mVenus/+; ; R72F11-Gal4/UAS-HMC02975* (yellow), and 20x*UAS-IVS-*
1077 *CsChrimson::mVenus/+; ; R72F11-Gal4/UAS-HMC03643* (orange). Genotypes in (B-D) are the
1078 same as mentioned here.
1079 (B) A violin plot of start of first rolling bout for each larva during stimulation. Statistics: Kruskal-
1080 Wallis test: H = 86.50, $p < 0.001$; Bonferroni-corrected Mann-Whitney U test, $p < 0.001$ for
1081 GABA-B-R1^2, GABA-B-R2, and GABA-A-R groups, n = 271, 194, 154, 178, 174 from left to
1082 right.
1083 (C) A violin plot of end of first rolling bout for each larva during stimulation. Statistics: Kruskal-
1084 Wallis test: H=36.01, $p < 0.001$; Bonferroni-corrected Mann-Whitney U test, $p < 0.001$ for GABA-
1085 B-R2 and GABA-A-R groups, n = 271, 194, 154, 178, 174 from left to right.
1086 (D) A violin plot of start of first crawling bout for each larva during stimulation. Statistics: Kruskal-
1087 Wallis test: H = 53.07, $p < 0.001$; Bonferroni-corrected Mann-Whitney U test, $p < 0.001$ for
1088 GABA-B-R1^2 group, n = 89, 119, 139, 135, 137 from left to right.
1089 (E) Calcium transients (mean ± s.e.m.) represented by $\Delta F/F_0$ are evoked in Basin axons by
1090 optogenetic activation of Basin neurons various intensities. N = 9. Genotype: *20xUAS-Syn21-*
1091 *opGCaMP6s,10xUAS-Syn21-CsChrimson88::tdTomato/+;CyO/+;TM6/R72F11-Gal4*.
1092 (F) Calcium transients (mean ± s.e.m.) in Basin axons represented by $\Delta F/F_0$ are decreased by
1093 optogenetic activation of SeIN128 neurons at various intensities. N = 10. Genotype: *20xUAS-*

Syn21-opGCaMP6s,10xUAS-Syn21-CsChrimson88::tdTomato/+;CyO/R54B01-Gal4.AD;R72F11-Gal4/R46E07-Gal4.DBD.

For (E) to (F), irradiances from left to right are 0.04, 0.1, 0.3, 0.5, and 1.4 μW/mm^2. For each irradiance, individual traces are shown with gray lines, whereas the average of individuals is shown in black. Shaded gray area denotes period of optogenetic activation (0 to 1 s).

$^{**}p < 0.01$, $^{***}p < 0.001$.

Figure 8. SeIN128 inhibits rolling elicited by both Basin-2 and Basin-4 activation

(A) Binned larval rolling probabilities during the first 5 s of stimulation. Error bars, 95% confidence interval. n = 81, 119. Statistics: Chi-square test, $\chi^2 = 35.51$, $p < 0.001$. Genotypes: *20xUAS-IVS-CsChrimson::mVenus/+; R72F11-Gal4.AD/+; R38H09-Gal4.DBD/+* (black); *20xUAS-IVS-CsChrimson::mVenus/+; R72F11-Gal4.AD/R54B01-Gal4.AD; R38H09-Gal4.DBD/R46E07-Gal4.DBD* (red). Genotypes in (B-D) are the same as mentioned here.

(B) Cumulative plot of rolling duration. Statistics: Mann-Whitney U test, $p = 0.0034$, n = 206, 83.

(C) A violin plot of end of first rolling bout for each larva during stimulation. Statistics: Mann-Whitney U test, $p = 0.0047$, n = 57, 38.

(D) A violin plot of start of first crawling bout for each larva during stimulation. Statistics: Mann-Whitney U test, $p = 0.045$, n = 107, 38.

(E) Binned larval rolling probabilities during first 5 s of stimulation. Error bars, 95% confidence interval. n = 192, 213. Statistics: Chi-square test, $\chi^2 = 64.81$, $p < 0.001$. Genotypes: *20xUAS-IVS-CsChrimson::mVenus/+; R72F11-Gal4.AD/+; R57F07-Gal4.DBD/+* (black); *20xUAS-IVS-CsChrimson::mVenus/+; R72F11-Gal4.AD/R54B01-Gal4.AD; R57F07-Gal4.DBD/R46E07-Gal4.DBD* (red). Genotypes in (F-H) are the same as mentioned here.

(F) Cumulative plot of rolling duration. Statistics: Mann-Whitney U test, $p = 0.032$, n = 231, 71.

(G) A violin plot of end of first rolling bout for each larva during stimulation. Statistics: Mann-Whitney U test, $p = 0.0047$, n = 129, 61.

(H) A violin plot of start of first crawling bout for each larva during stimulation. Statistics: Mann-Whitney U test, $p < 0.001$, n = 159, 71.

(I) A summarizing illustration. Basin-2 activates rolling and supresses fast crawling, while SeIN128 decreases Basin-2 activities to inhibit rolling and disinhibit fast crawling. Arrows show activation and blunt ends represent inhibition.

1125 $^{**}p < 0.01$, $^{***}p < 0.001$.

1126

1127 **Figure 8 - Figure supplement 1. SeIN128 inhibits rolling elicited by both Basin-2 and Basin-**
1128 **4 activation.**

1129 (A) and (B) show ethograms of Basin-2 activation (A) and Basin-4 activation (B). Each row
1130 represents an individual larva. Pink, blue, green, orange, and purple lines represent bouts of rolling,
1131 turning, crawling, backward crawling, and hunching. The red bar and dashed lines denote the time
1132 window during the period of neural activation. Genotypes: *20xUAS-IVS-CsChrimson::mVenus/+;*
1133 *R72F11-Gal4.AD/+; R38H09-Gal4.DBD/+* (A); *20xUAS-IVS-CsChrimson::mVenus/+; R72F11-*
1134 *Gal4.AD/+; R57F07-Gal4.DBD/+* (B). Genotypes in (C) are the same as mentioned here.

1135 (C) Cumulative plot of rolling duration. Statistics: Mann-Whitney U test, $p < 0.001$, n = 681, 141.

1136 (D) Time series of rolling probabilities of larvae with Basin-2 activation (black), or SS04185 and
1137 Basin-2 coactivation (red). The red bar and dashed lines display the window of optogenetic
1138 stimulation eliciting larval escape responses. Shaded areas show 95% confidential intervals of
1139 rolling probabilities. Genotypes: *20xUAS-IVS-CsChrimson::mVenus/+; R72F11-Gal4.AD/+;*
1140 *R38H09-Gal4.DBD/+* (black); *20xUAS-IVS-CsChrimson::mVenus/+; R72F11-Gal4.AD/R54B01-*
1141 *Gal4.AD; R38H09-Gal4.DBD/R46E07-Gal4.DBD* (red). Genotypes in (E) are the same as
1142 mentioned here.

1143 (E) A violin plot of start of first rolling bout for each larva during stimulation. Statistics: Mann-
1144 Whitney U test, $p < 0.001$, n = 57, 38.

1145 (F) Time series of rolling probabilities of larvae with Basin-4 activation (black), or SS04185 and
1146 Basin-4 coactivation (red). The red bar and dashed lines display the window of optogenetic
1147 stimulation eliciting larval escape responses. Shaded areas show 95% confidential intervals of
1148 rolling probabilities. Genotypes: *20xUAS-IVS-CsChrimson::mVenus/+; R72F11-Gal4.AD/+;*
1149 *R57F07-Gal4.DBD/+* (black); *20xUAS-IVS-CsChrimson::mVenus/+; R72F11-Gal4.AD/R54B01-*
1150 *Gal4.AD; R57F07-Gal4.DBD/R46E07-Gal4.DBD* (red). Genotypes in (G) are the same as
1151 mentioned here.

1152 (G) A violin plot of start of first rolling bout for each larva during stimulation. Statistics: Mann-
1153 Whitney U test, $p > 0.05$, n = 129, 61. $^{**}p < 0.01$, $^{***}p < 0.001$.

1154

References

Banerjee, S., Vernon, S., Jiao, W., Choi, B. J., Ruchti, E., Asadzadeh, J., Burri, O., Stowers, R. S., & McCabe, B. D. (2021). Miniature neurotransmission is required to maintain Drosophila synaptic structures during ageing. *Nat Commun*, *12*(1), 4399. https://doi.org/10.1038/s41467-021-24490-1

Burgos, A., Honjo, K., Ohyama, T., Qian, C. S., Shin, G. J., Gohl, D. M., Silies, M., Tracey, W. D., Zlatic, M., Cardona, A., & Grueber, W. B. (2018). Nociceptive interneurons control modular motor pathways to promote escape behavior in Drosophila. *Elife*, *7*. https://doi.org/10.7554/eLife.26016

Burrell, B. D. (2017). Comparative biology of pain: What invertebrates can tell us about how nociception works. *J Neurophysiol*, *117*(4), 1461-1473. https://doi.org/10.1152/jn.00600.2016

Campagner, D., Vale, R., Tan, Y. L., Iordanidou, P., Pavon Arocas, O., Claudi, F., Stempel, A. V., Keshavarzi, S., Petersen, R. S., Margrie, T. W., & Branco, T. (2023). A cortico-collicular circuit for orienting to shelter during escape. *Nature*, *613*(7942), 111-119. https://doi.org/10.1038/s41586-022-05553-9

Cattaert, D., & El Manira, A. (1999). Shunting versus inactivation: analysis of presynaptic inhibitory mechanisms in primary afferents of the crayfish. *J Neurosci*, *19*(14), 6079-6089. https://doi.org/10.1523/JNEUROSCI.19-14-06079.1999

Chalfie, M., & Sulston, J. (1981). Developmental genetics of the mechanosensory neurons of Caenorhabditis elegans. *Dev Biol*, *82*(2), 358-370. https://doi.org/10.1016/0012-1606(81)90459-0

Chalfie, M., Sulston, J. E., White, J. G., Southgate, E., Thomson, J. N., & Brenner, S. (1985). The neural circuit for touch sensitivity in Caenorhabditis elegans. *J Neurosci*, *5*(4), 956-964. https://doi.org/10.1523/JNEUROSCI.05-04-00956.1985

Chin, M. R., & Tracey, W. D., Jr. (2017). Nociceptive Circuits: Can't Escape Detection. *Curr Biol*, *27*(16), R796-R798. https://doi.org/10.1016/j.cub.2017.07.031

Cooney, P. C., Huang, Y., Li, W., Perera, D. M., Hormigo, R., Tabachnik, T., Godage, I. S., Hillman, E. M. C., Grueber, W. B., & Zarin, A. A. (2023). Neuromuscular basis of Drosophila larval rolling escape behavior. *Proc Natl Acad Sci U S A*, *120*(51), e2303641120. https://doi.org/10.1073/pnas.2303641120

Dason, J. S., Cheung, A., Anreiter, I., Montemurri, V. A., Allen, A. M., & Sokolowski, M. B. (2020). Drosophila melanogaster foraging regulates a nociceptive-like escape behavior through a developmentally plastic sensory circuit. *Proc Natl Acad Sci U S A*, *117*(38), 23286-23291. https://doi.org/10.1073/pnas.1820840116

Dolan, M. J., Luan, H., Shropshire, W. C., Sutcliffe, B., Cocanougher, B., Scott, R. L., Frechter, S., Zlatic, M., Jefferis, G., & White, B. H. (2017). Facilitating Neuron-Specific Genetic Manipulations in Drosophila melanogaster Using a Split GAL4 Repressor. *Genetics*, *206*(2), 775-784. https://doi.org/10.1534/genetics.116.199687

Fei, H., Chow, D. M., Chen, A., Romero-Calderon, R., Ong, W. S., Ackerson, L. C., Maidment, N. T., Simpson, J. H., Frye, M. A., & Krantz, D. E. (2010). Mutation of the Drosophila vesicular GABA transporter disrupts visual figure detection. *J Exp Biol*, *213*(Pt 10), 1717-1730. https://doi.org/10.1242/jeb.036053

Guo, D., & Hu, J. (2014). Spinal presynaptic inhibition in pain control. *Neuroscience*, *283*, 95-106. https://doi.org/10.1016/j.neuroscience.2014.09.032

Hu, C., Petersen, M., Hoyer, N., Spitzweck, B., Tenedini, F., Wang, D., Gruschka, A., Burchardt, L. S., Szpotowicz, E., Schweizer, M., Guntur, A. R., Yang, C. H., & Soba, P. (2017). Sensory integration and neuromodulatory feedback facilitate Drosophila mechanonociceptive behavior. *Nat Neurosci*, *20*(8), 1085-1095. https://doi.org/10.1038/nn.4580

Hu, Y., Wang, C., Yang, L., Pan, G., Liu, H., Yu, G., & Ye, B. (2020). A Neural Basis for Categorizing Sensory Stimuli to Enhance Decision Accuracy. *Curr Biol*, *30*(24), 4896-4909 e4896. https://doi.org/10.1016/j.cub.2020.09.045

Hwang, R. Y., Zhong, L., Xu, Y., Johnson, T., Zhang, F., Deisseroth, K., & Tracey, W. D. (2007). Nociceptive neurons protect Drosophila larvae from parasitoid wasps. *Curr Biol*, *17*(24), 2105-2116. https://doi.org/10.1016/j.cub.2007.11.029

Im, S. H., & Galko, M. J. (2012). Pokes, sunburn, and hot sauce: Drosophila as an emerging model for the biology of nociception. *Dev Dyn*, *241*(1), 16-26. https://doi.org/10.1002/dvdy.22737

Imambocus, B. N., Zhou, F., Formozov, A., Wittich, A., Tenedini, F. M., Hu, C., Sauter, K., Macarenhas Varela, E., Heredia, F., Casimiro, A. P., Macedo, A., Schlegel, P., Yang, C. H., Miguel-Aliaga, I., Wiegert, J. S., Pankratz, M. J., Gontijo, A. M., Cardona, A., & Soba, P. (2022). A neuropeptidergic circuit gates selective escape behavior of Drosophila larvae. *Curr Biol*, *32*(1), 149-163 e148. https://doi.org/10.1016/j.cub.2021.10.069

Isaacson, J. S., & Scanziani, M. (2011). How inhibition shapes cortical activity. *Neuron*, *72*(2), 231-243. https://doi.org/10.1016/j.neuron.2011.09.027

Kabra, M., Robie, A. A., Rivera-Alba, M., Branson, S., & Branson, K. (2013). JAABA: interactive machine learning for automatic annotation of animal behavior. *Nat Methods*, *10*(1), 64-67. https://doi.org/10.1038/nmeth.2281

Kaneko, T., Macara, A. M., Li, R., Hu, Y., Iwasaki, K., Dunnings, Z., Firestone, E., Horvatic, S., Guntur, A., Shafer, O. T., Yang, C. H., Zhou, J., & Ye, B. (2017). Serotonergic Modulation Enables Pathway-Specific Plasticity in a Developing Sensory Circuit in Drosophila. *Neuron*, *95*(3), 722. https://doi.org/10.1016/j.neuron.2017.07.023

Kapfer, C., Glickfeld, L. L., Atallah, B. V., & Scanziani, M. (2007). Supralinear increase of recurrent inhibition during sparse activity in the somatosensory cortex. *Nat Neurosci*, *10*(6), 743-753. https://doi.org/10.1038/nn1909

Kohsaka, H. (2023). Linking neural circuits to the mechanics of animal behavior in Drosophila larval locomotion. *Front Neural Circuits*, *17*, 1175899. https://doi.org/10.3389/fncir.2023.1175899

Manoim, J. E., Davidson, A. M., Weiss, S., Hige, T., & Parnas, M. (2022). Lateral axonal modulation is required for stimulus-specific olfactory conditioning in Drosophila. *Curr Biol*, *32*(20), 4438-4450 e4435. https://doi.org/10.1016/j.cub.2022.09.007

Masson, J. B., Laurent, F., Cardona, A., Barre, C., Skatchkovsky, N., Zlatic, M., & Jovanic, T. (2020). Identifying neural substrates of competitive interactions and sequence transitions during mechanosensory responses in Drosophila. *PLoS Genet*, *16*(2), e1008589. https://doi.org/10.1371/journal.pgen.1008589

McGann, J. P. (2013). Presynaptic inhibition of olfactory sensory neurons: new mechanisms and potential functions. *Chem Senses*, *38*(6), 459-474. https://doi.org/10.1093/chemse/bjt018

Nakamizo-Dojo, M., Ishii, K., Yoshino, J., Tsuji, M., & Emoto, K. (2023). Descending GABAergic pathway links brain sugar-sensing to peripheral nociceptive gating in Drosophila. *Nat Commun*, *14*(1), 6515. https://doi.org/10.1038/s41467-023-42202-9

Nern, A., Pfeiffer, B. D., & Rubin, G. M. (2015). Optimized tools for multicolor stochastic labeling reveal diverse stereotyped cell arrangements in the fly visual system. *Proc Natl Acad Sci U S A*, *112*(22), E2967-2976. https://doi.org/10.1073/pnas.1506763112

Ohyama, T., Jovanic, T., Denisov, G., Dang, T. C., Hoffmann, D., Kerr, R. A., & Zlatic, M. (2013). High-throughput analysis of stimulus-evoked behaviors in Drosophila larva reveals multiple modality-specific escape strategies. *PLoS One*, *8*(8), e71706. https://doi.org/10.1371/journal.pone.0071706

Ohyama, T., Schneider-Mizell, C. M., Fetter, R. D., Aleman, J. V., Franconville, R., Rivera-Alba, M., Mensh, B. D., Branson, K. M., Simpson, J. H., Truman, J. W., Cardona, A., & Zlatic, M. (2015). A multilevel multimodal circuit enhances action selection in Drosophila. *Nature*, *520*(7549), 633-639. https://doi.org/10.1038/nature14297

Oikawa, I., Kondo, S., Hashimoto, K., Yoshida, A., Hamajima, M., Tanimoto, H., Furukubo-Tokunaga, K., & Honjo, K. (2023). A descending inhibitory mechanism of nociception mediated by an evolutionarily conserved neuropeptide system in Drosophila. *Elife*, *12*. https://doi.org/10.7554/eLife.85760

Oleson, E. B., Beckert, M. V., Morra, J. T., Lansink, C. S., Cachope, R., Abdullah, R. A., Loriaux, A. L., Schetters, D., Pattij, T., Roitman, M. F., Lichtman, A. H., & Cheer, J. F. (2012). Endocannabinoids shape accumbal encoding of cue-motivated behavior via CB1 receptor activation in the ventral tegmentum. *Neuron*, *73*(2), 360-373. https://doi.org/10.1016/j.neuron.2011.11.018

Onodera, K., Baba, S., Murakami, A., Uemura, T., & Usui, T. (2017). Small conductance Ca(2+)-activated K(+) channels induce the firing pause periods during the activation of Drosophila nociceptive neurons. *Elife*, *6*. https://doi.org/10.7554/eLife.29754

Palay, S. L. (1956). Synapses in the central nervous system. *J Biophys Biochem Cytol*, *2*(4 Suppl), 193-202. https://doi.org/10.1083/jcb.2.4.193

Pan-Vazquez, A., Wefelmeyer, W., Gonzalez Sabater, V., Neves, G., & Burrone, J. (2020). Activity-Dependent Plasticity of Axo-axonic Synapses at the Axon Initial Segment. *Neuron*, *106*(2), 265-276 e266. https://doi.org/10.1016/j.neuron.2020.01.037

Papadopoulou, M., Cassenaer, S., Nowotny, T., & Laurent, G. (2011). Normalization for sparse encoding of odors by a wide-field interneuron. *Science*, *332*(6030), 721-725. https://doi.org/10.1126/science.1201835

Patel, N. H. (1994). Imaging neuronal subsets and other cell types in whole-mount Drosophila embryos and larvae using antibody probes. *Methods Cell Biol*, *44*, 445-487. https://doi.org/10.1016/s0091-679x(08)60927-9

Peirs, C., & Seal, R. P. (2016). Neural circuits for pain: Recent advances and current views. *Science*, *354*(6312), 578-584. https://doi.org/10.1126/science.aaf8933

Pinault, D., Smith, Y., & Deschenes, M. (1997). Dendrodendritic and axoaxonic synapses in the thalamic reticular nucleus of the adult rat. *J Neurosci*, *17*(9), 3215-3233. https://doi.org/10.1523/JNEUROSCI.17-09-03215.1997

Ray, S., Aldworth, Z. N., & Stopfer, M. A. (2020). Feedback inhibition and its control in an insect olfactory circuit. *Elife*, *9*. https://doi.org/10.7554/eLife.53281

Schneider-Mizell, C. M., Bodor, A. L., Collman, F., Brittain, D., Bleckert, A., Dorkenwald, S., Turner, N. L., Macrina, T., Lee, K., Lu, R., Wu, J., Zhuang, J., Nandi, A., Hu, B., Buchanan, J., Takeno, M. M., Torres, R., Mahalingam, G., Bumbarger, D. J., . . . Costa, N. M. D. (2021). Structure and function of axo-axonic inhibition. *Elife*, *10*. https://doi.org/10.7554/eLife.73783

Stokes, C. C., & Isaacson, J. S. (2010). From dendrite to soma: dynamic routing of inhibition by complementary interneuron microcircuits in olfactory cortex. *Neuron*, *67*(3), 452-465. https://doi.org/10.1016/j.neuron.2010.06.029

Swierczek, N. A., Giles, A. C., Rankin, C. H., & Kerr, R. A. (2011). High-throughput behavioral analysis in C. elegans. *Nat Methods*, *8*(7), 592-598. https://doi.org/10.1038/nmeth.1625

Takagi, S., Cocanougher, B. T., Niki, S., Miyamoto, D., Kohsaka, H., Kazama, H., Fetter, R. D., Truman, J. W., Zlatic, M., Cardona, A., & Nose, A. (2017). Divergent Connectivity of Homologous Command-like Neurons Mediates Segment-Specific Touch Responses in Drosophila. *Neuron*, *96*(6), 1373-1387 e1376. https://doi.org/10.1016/j.neuron.2017.10.030

Tracey, W. D., Jr., Wilson, R. I., Laurent, G., & Benzer, S. (2003). painless, a Drosophila gene essential for nociception. *Cell*, *113*(2), 261-273. https://doi.org/10.1016/s0092-8674(03)00272-1

Veres, J. M., Fekete, Z., Muller, K., Andrasi, T., Rovira-Esteban, L., Barabas, B., Papp, O. I., & Hajos, N. (2023). Fear learning and aversive stimuli differentially change excitatory synaptic transmission in perisomatic inhibitory cells of the basal amygdala. *Front Cell Neurosci*, *17*, 1120338. https://doi.org/10.3389/fncel.2023.1120338

Vogt, K., Aso, Y., Hige, T., Knapek, S., Ichinose, T., Friedrich, A. B., Turner, G. C., Rubin, G. M., & Tanimoto, H. (2016). Direct neural pathways convey distinct visual information to Drosophila mushroom bodies. *Elife*, *5*. https://doi.org/10.7554/eLife.14009

Winding, M., Pedigo, B. D., Barnes, C. L., Patsolic, H. G., Park, Y., Kazimiers, T., Fushiki, A., Andrade, I. V., Khandelwal, A., Valdes-Aleman, J., Li, F., Randel, N., Barsotti, E., Correia, A., Fetter, R. D., Hartenstein, V., Priebe, C. E., Vogelstein, J. T., Cardona, A., & Zlatic, M. (2023). The connectome of an insect brain. *Science*, *379*(6636), eadd9330. https://doi.org/10.1126/science.add9330

Yoshimura, Y., & Callaway, E. M. (2005). Fine-scale specificity of cortical networks depends on inhibitory cell type and connectivity. *Nat Neurosci*, *8*(11), 1552-1559. https://doi.org/10.1038/nn1565

Yoshino, J., Morikawa, R. K., Hasegawa, E., & Emoto, K. (2017). Neural Circuitry that Evokes Escape Behavior upon Activation of Nociceptive Sensory Neurons in Drosophila Larvae. *Curr Biol*, *27*(16), 2499-2504 e2493. https://doi.org/10.1016/j.cub.2017.06.068

Zarin, A. A., Mark, B., Cardona, A., Litwin-Kumar, A., & Doe, C. Q. (2019). A multilayer circuit architecture for the generation of distinct locomotor behaviors in Drosophila. *Elife*, *8*. https://doi.org/10.7554/eLife.51781

Zheng, Z., Lauritzen, J. S., Perlman, E., Robinson, C. G., Nichols, M., Milkie, D., Torrens, O., Price, J., Fisher, C. B., Sharifi, N., Calle-Schuler, S. A., Kmecova, L., Ali, I. J., Karsh, B., Trautman, E. T., Bogovic, J. A., Hanslovsky, P., Jefferis, G., Kazhdan, M., . . . Bock, D. D. (2018). A Complete Electron Microscopy Volume of the Brain of Adult Drosophila melanogaster. *Cell*, *174*(3), 730-743 e722. https://doi.org/10.1016/j.cell.2018.06.019

J. Zhu et al., Figure 1

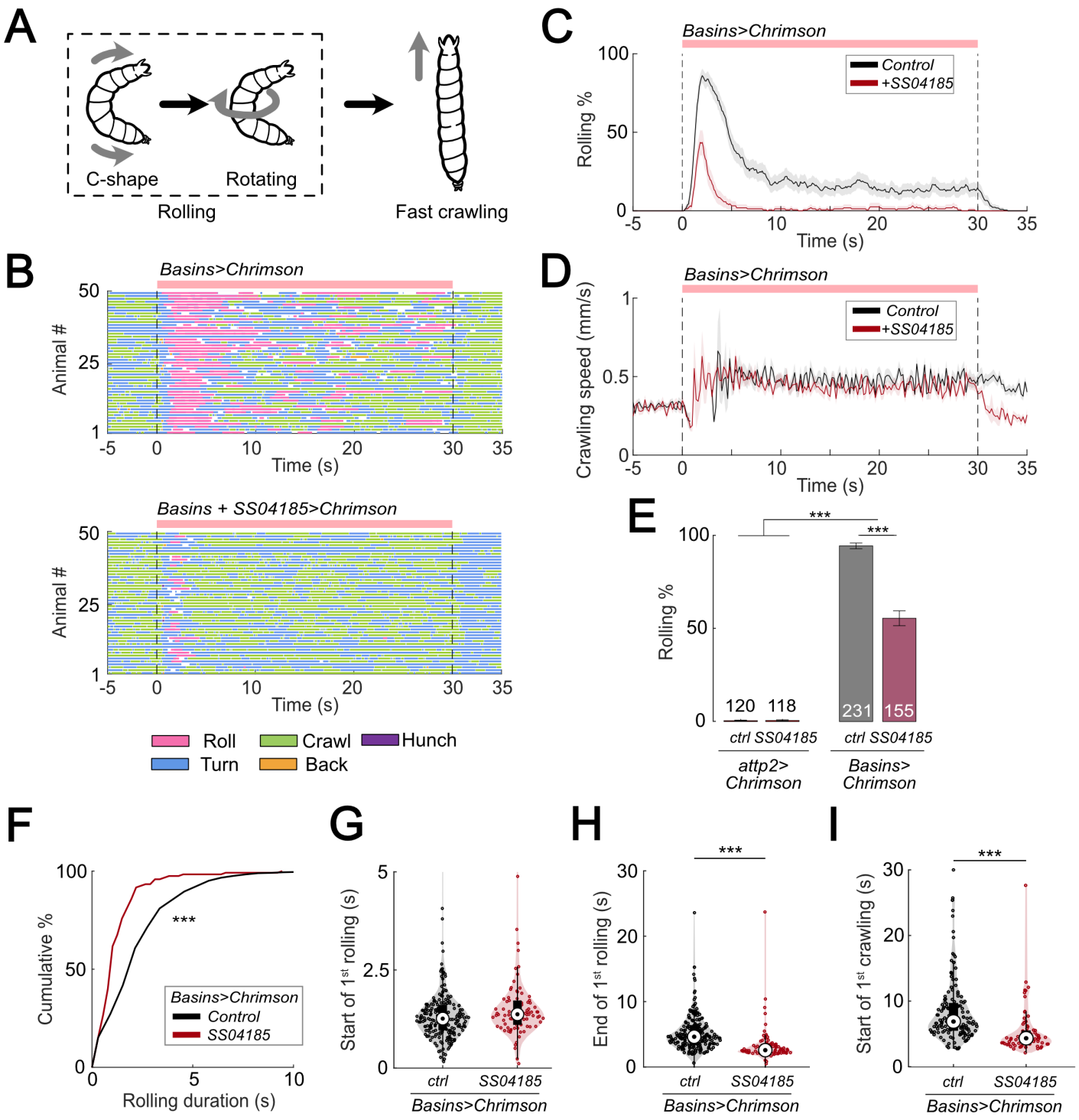

J. Zhu et al., Figure 1 - Figure supplement 1

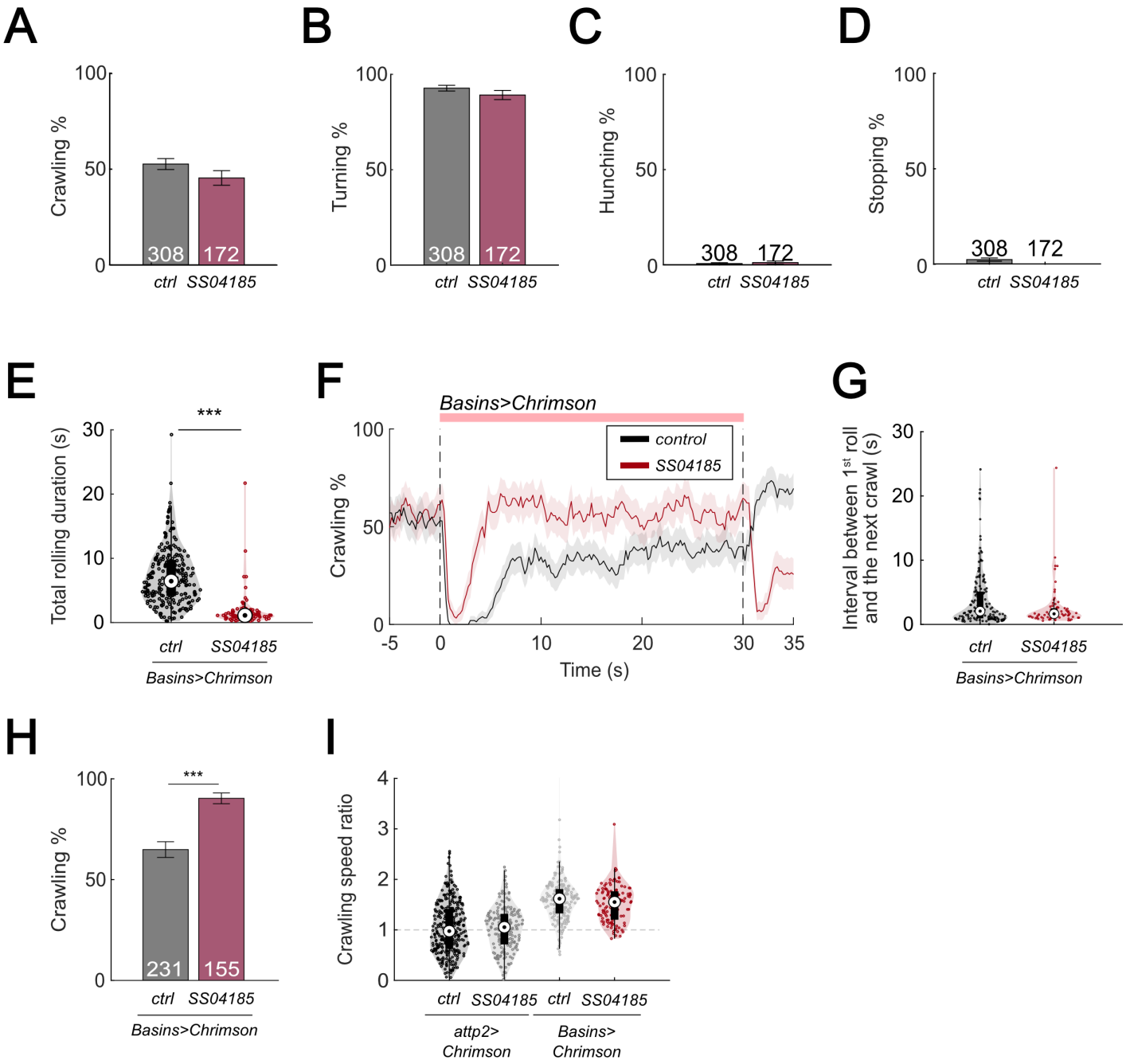

J. Zhu et al., Figure 1 - Figure supplement 2

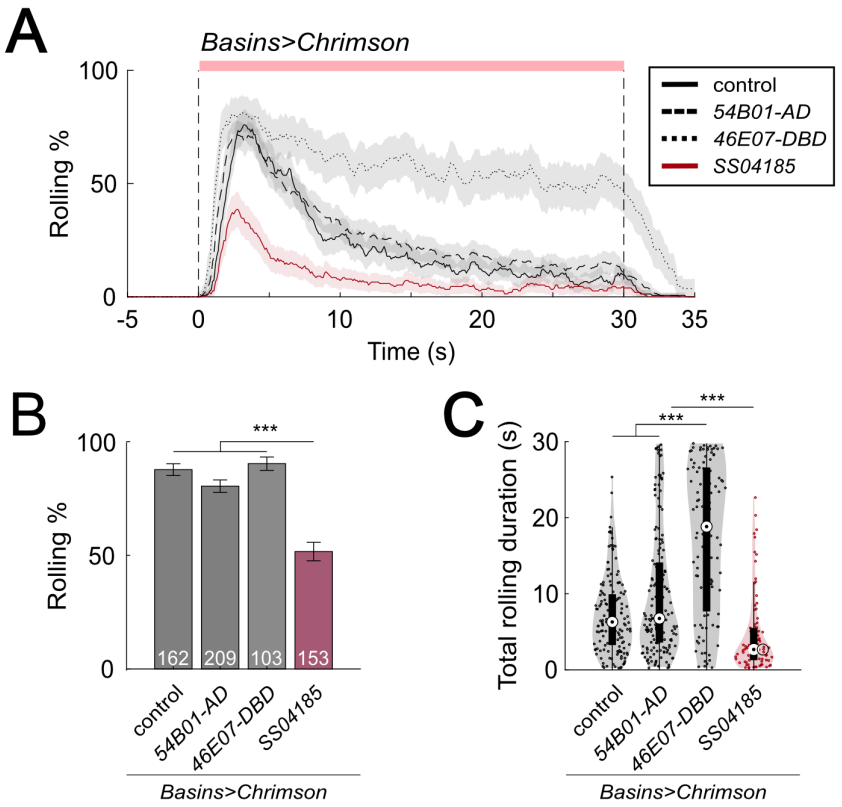

J. Zhu et al., Figure 2

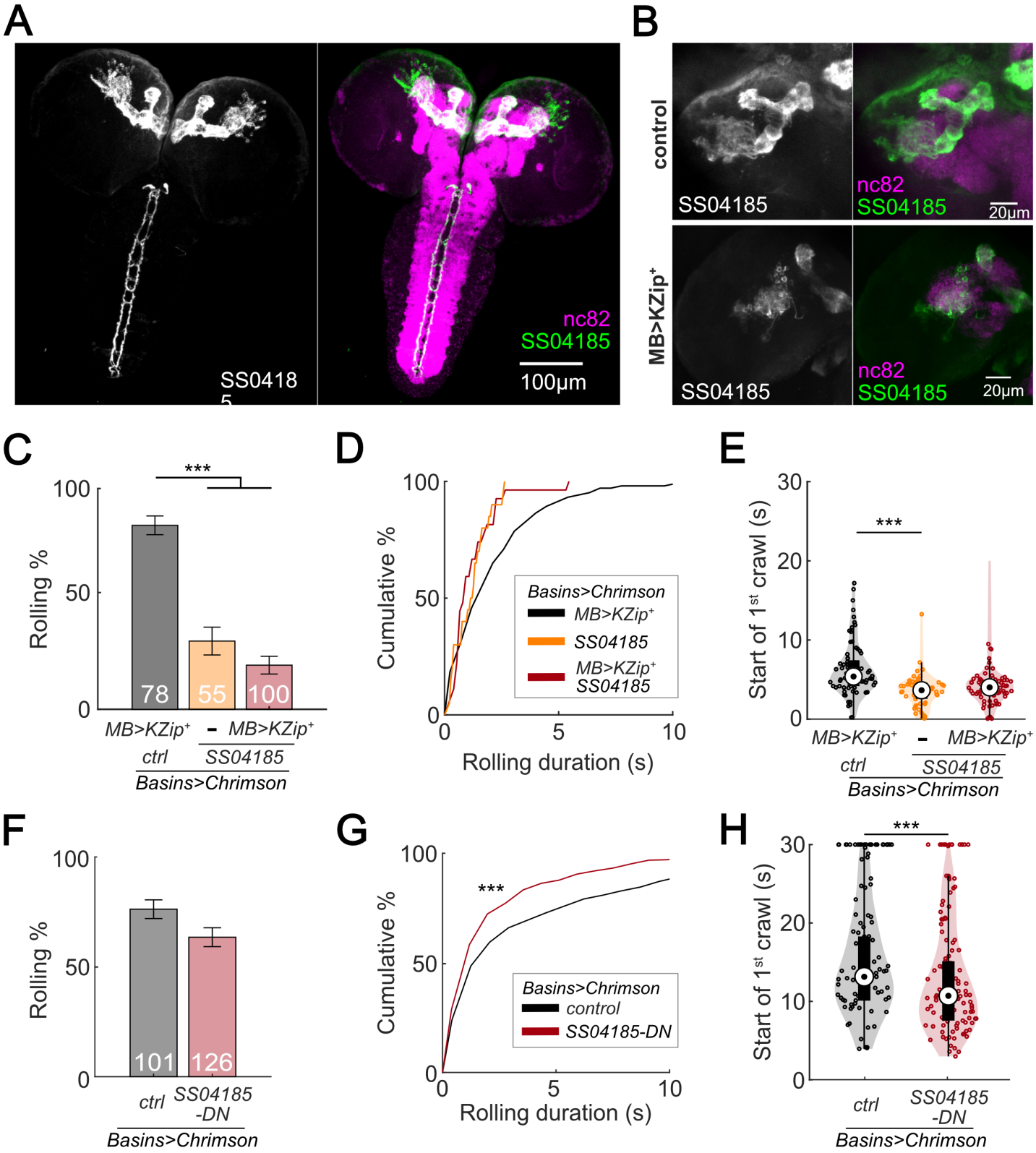

J. Zhu et al., Figure 2 - Figure supplement 1

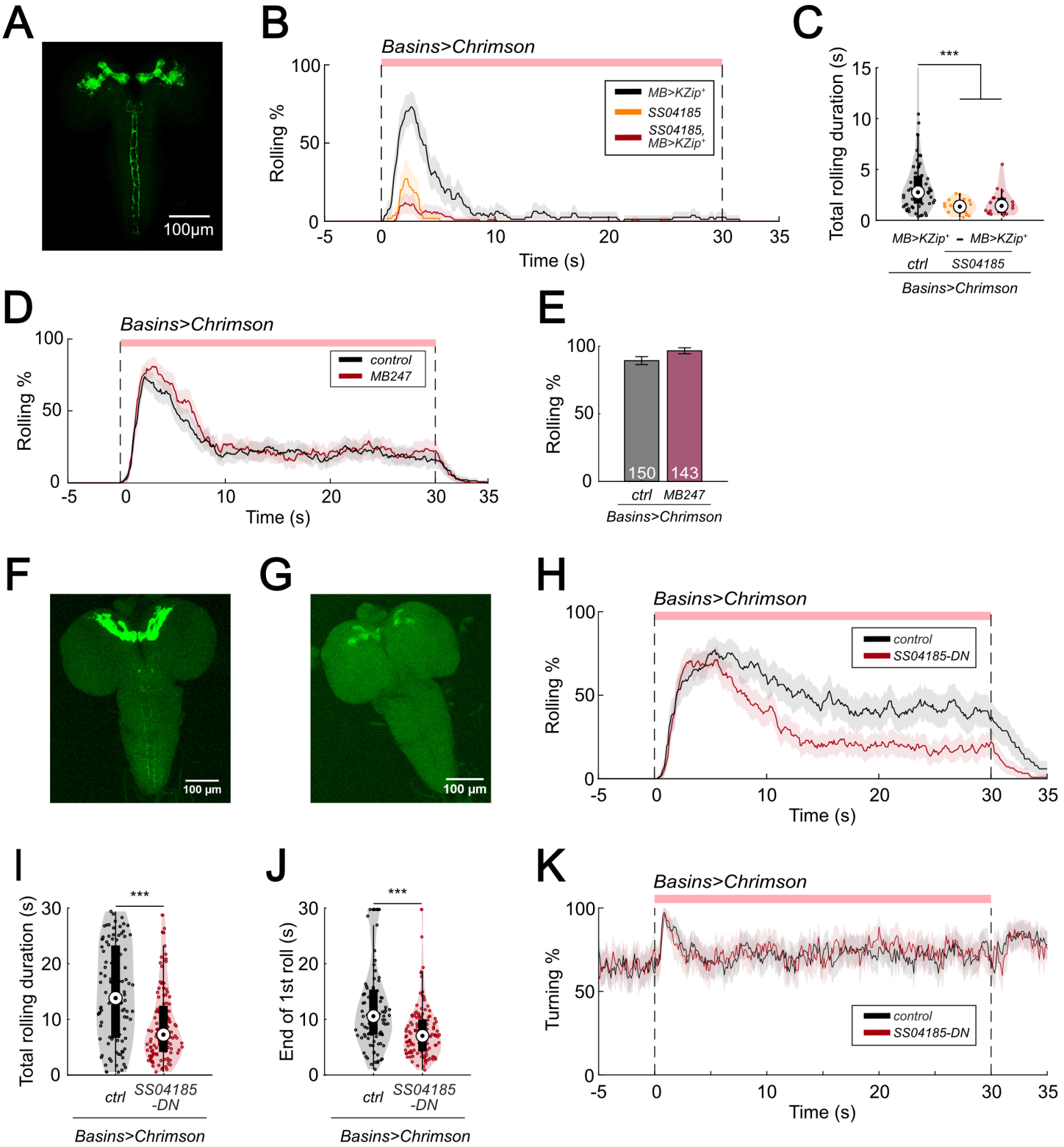

J. Zhu et al., Figure 3

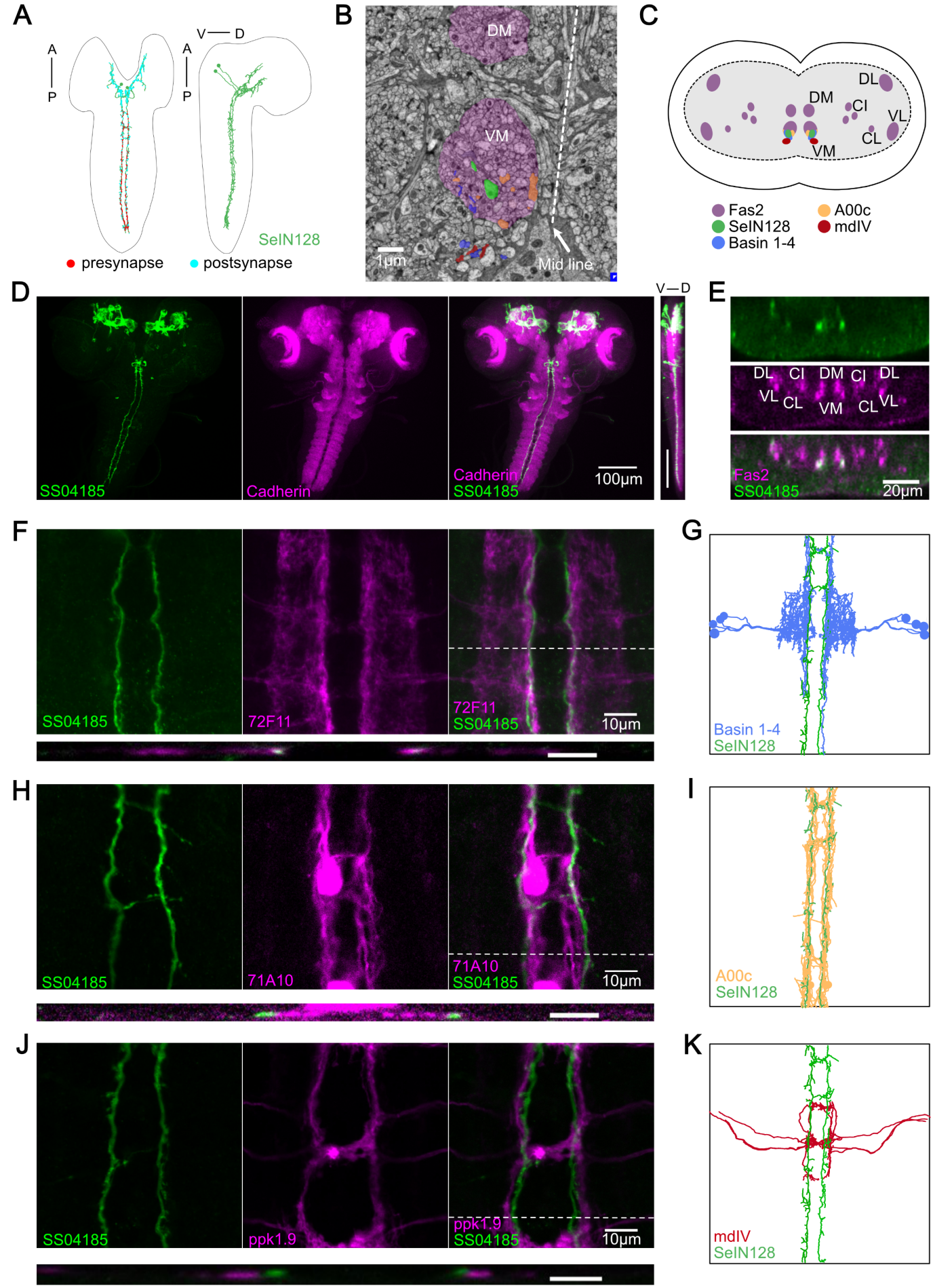

J. Zhu et al., Figure 4

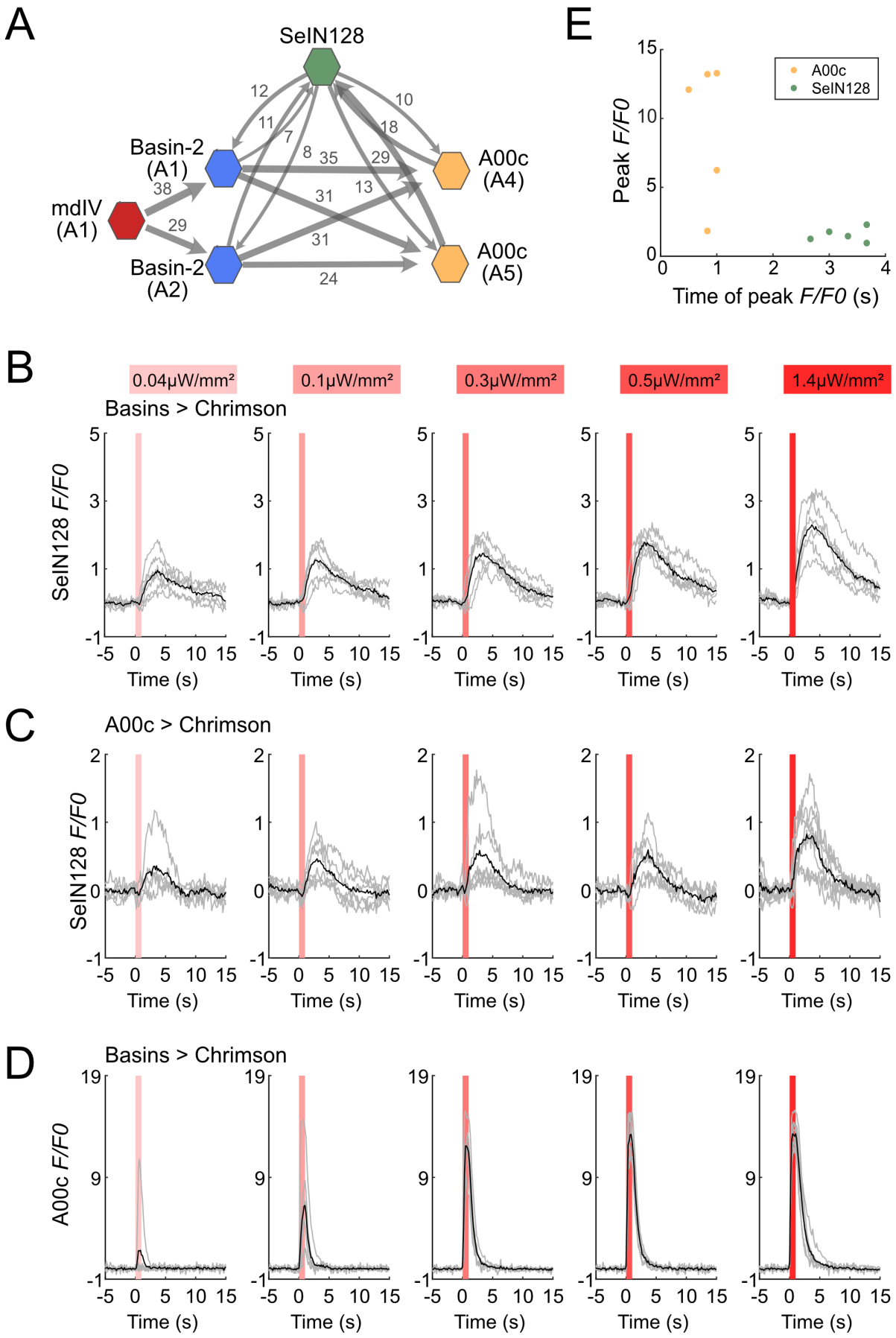

J. Zhu et al., Figure 4 - Figure supplement 1

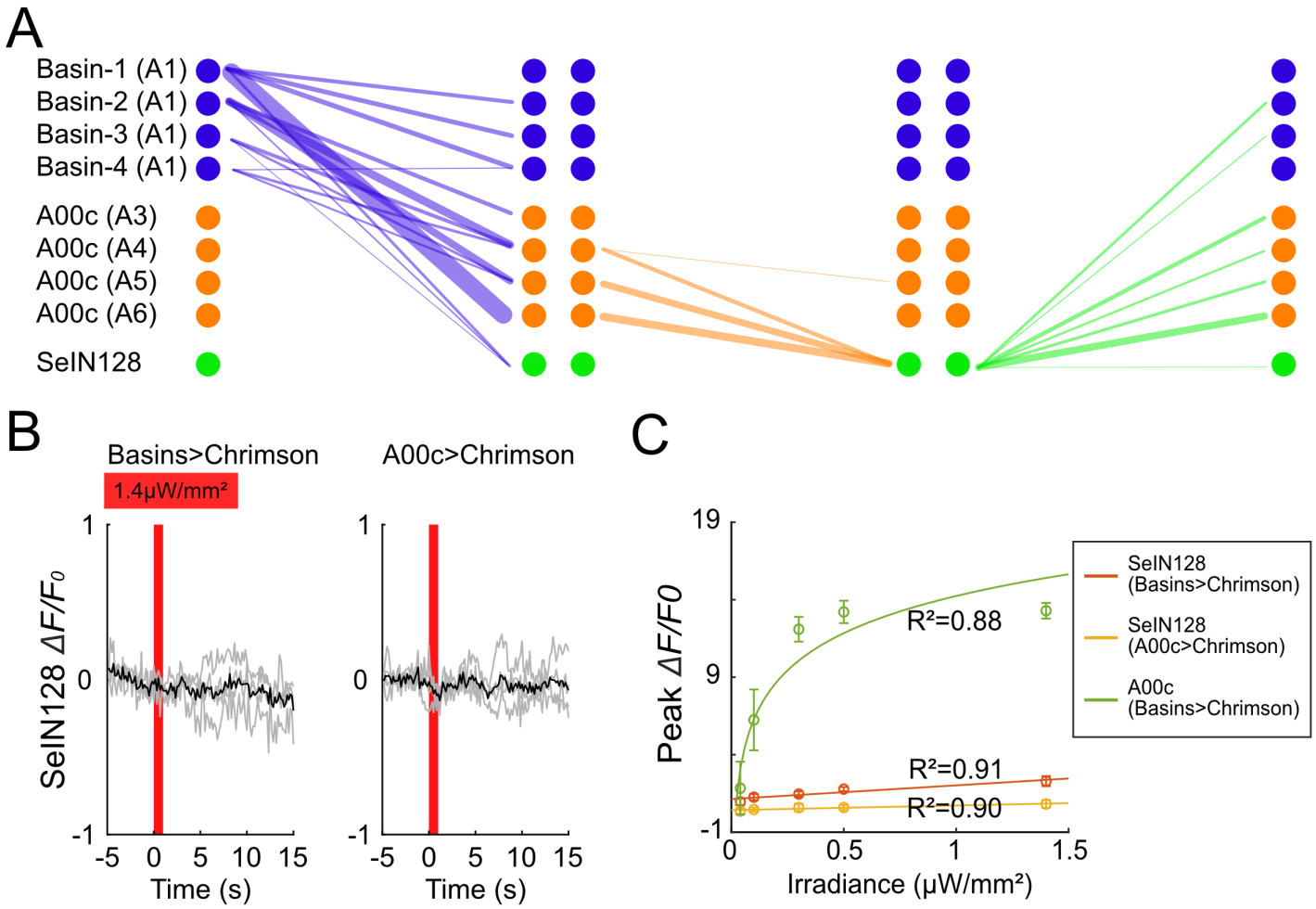

J. Zhu et al., Figure 4 - Figure supplement 2

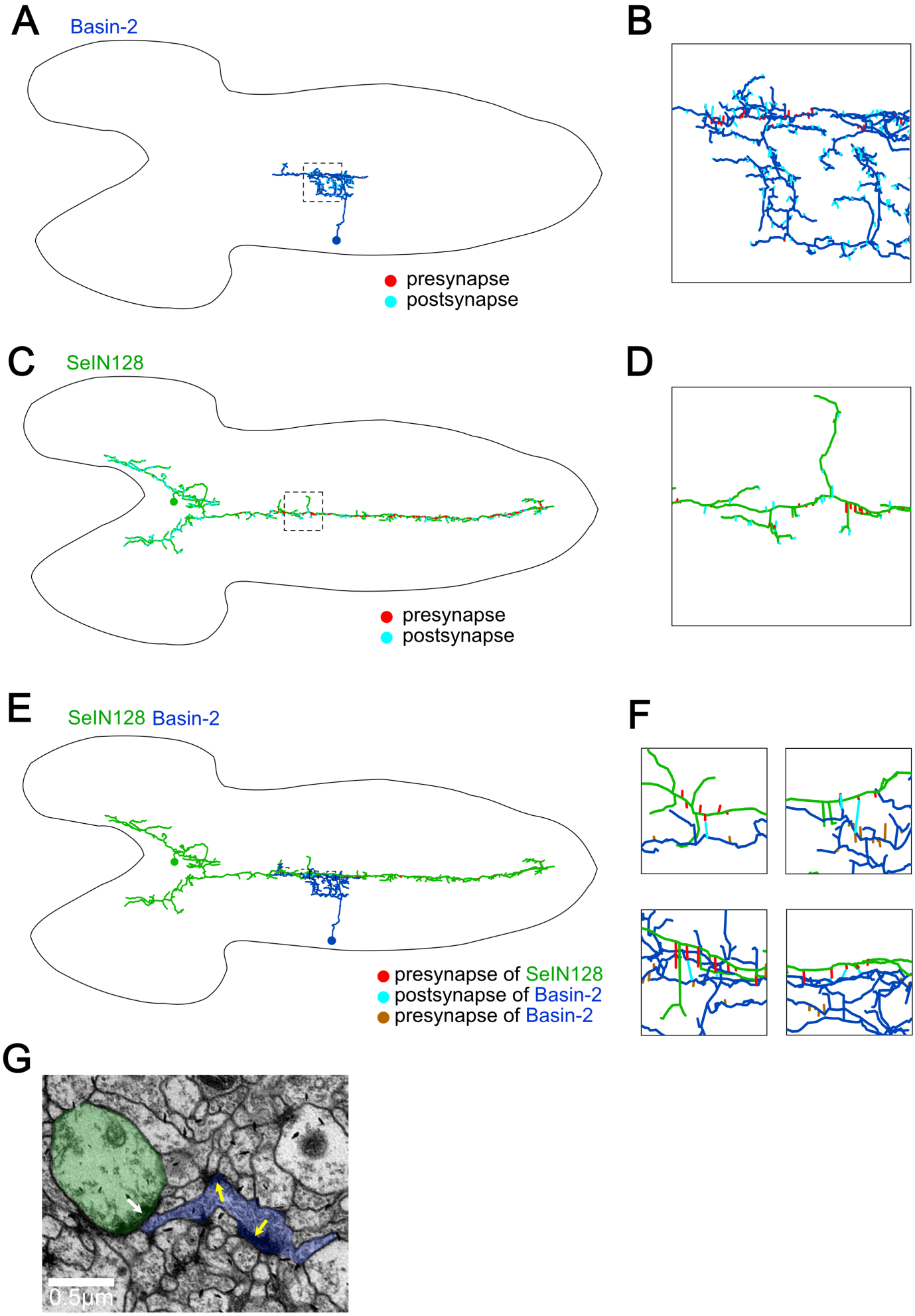

J. Zhu et al., Figure 5

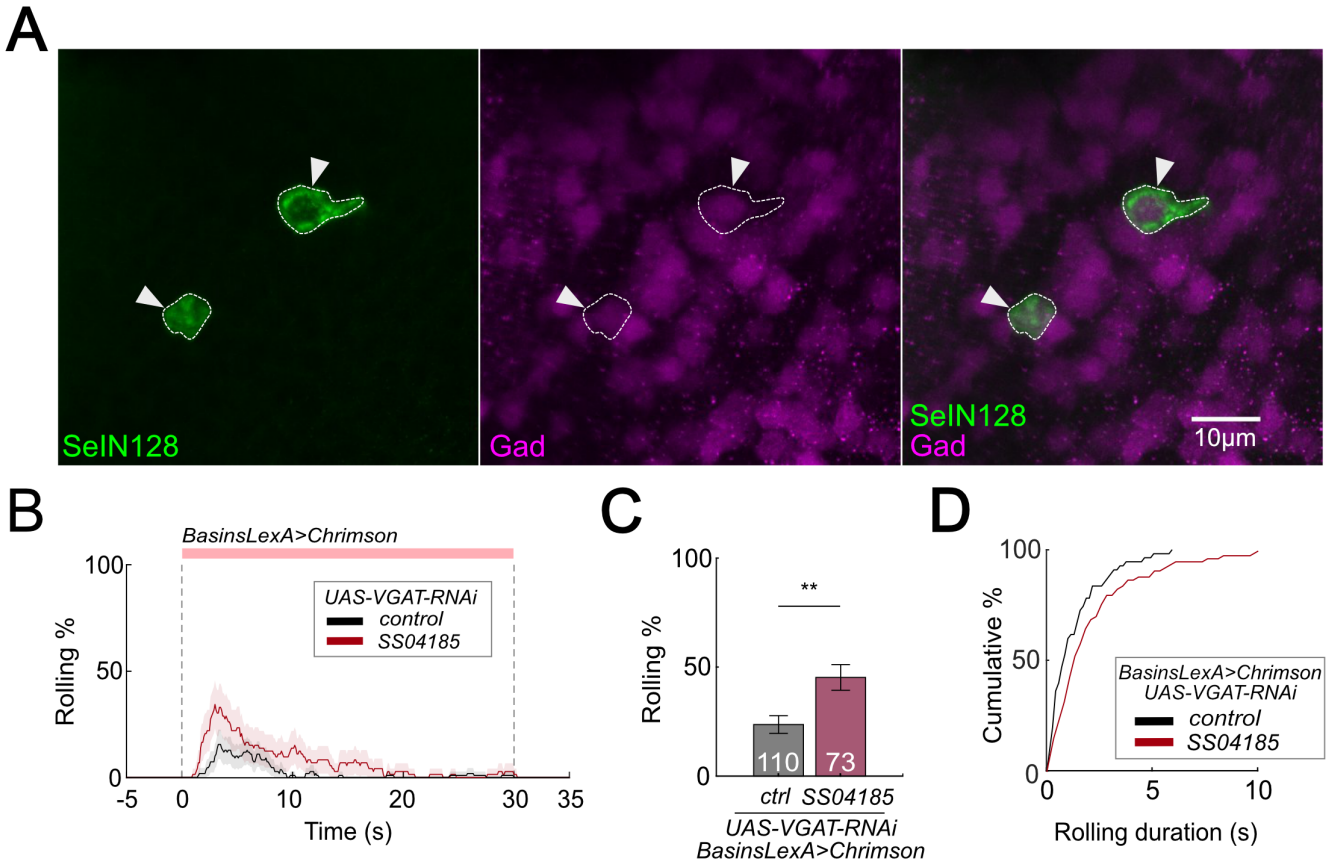

J. Zhu et al., Figure 5 - Figure supplement 1

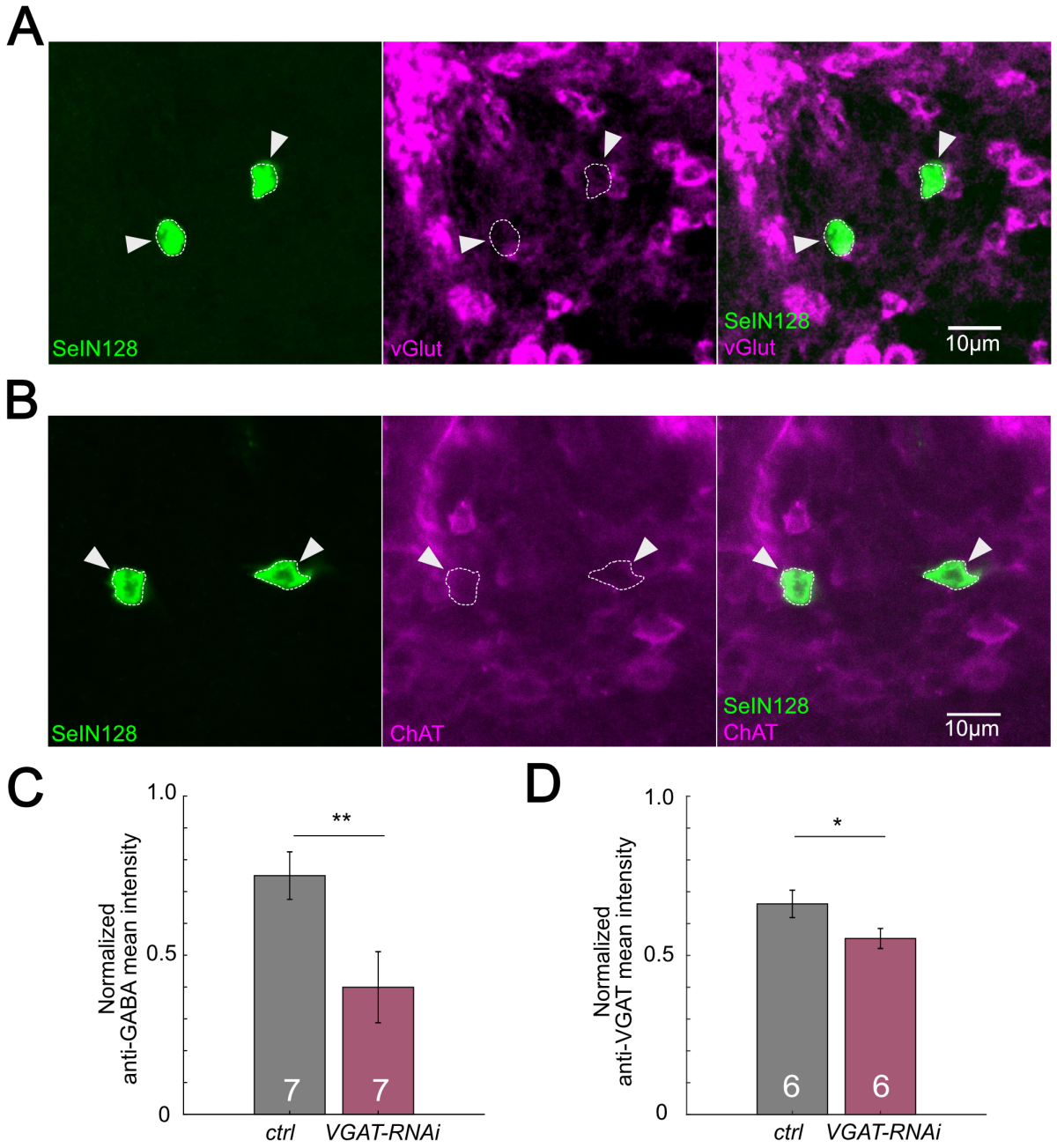

J. Zhu et al., Figure 6

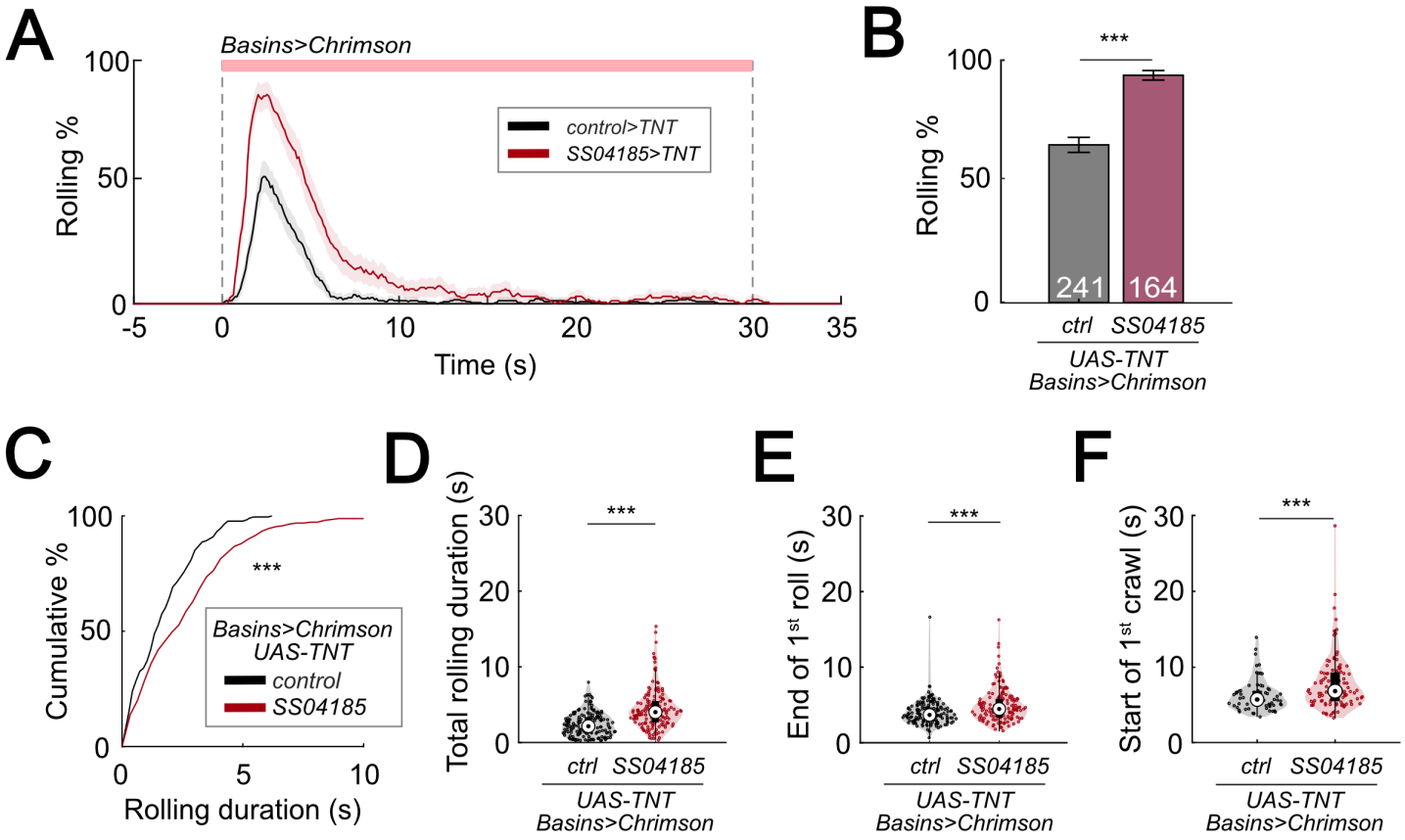

J. Zhu et al., Figure 6 - Figure supplement 1

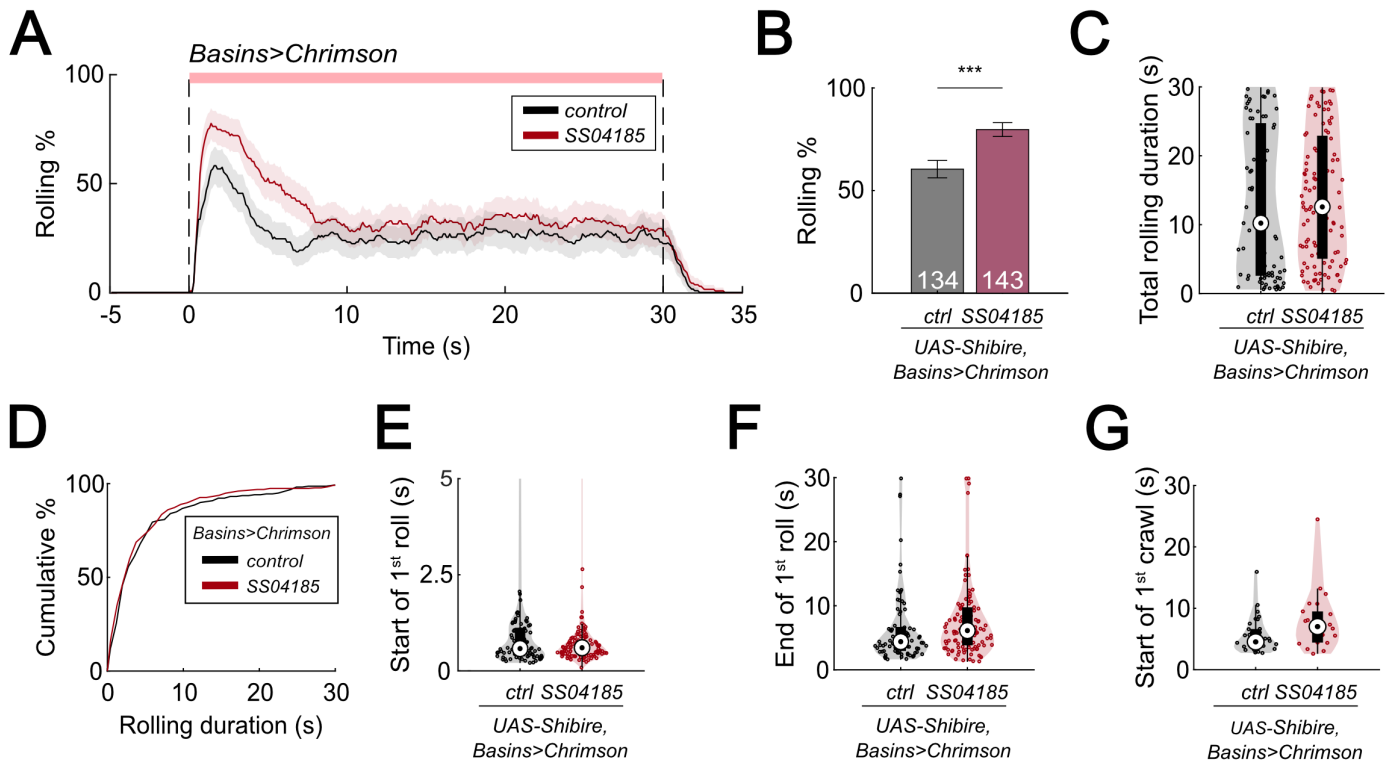

J. Zhu et al., Figure 7

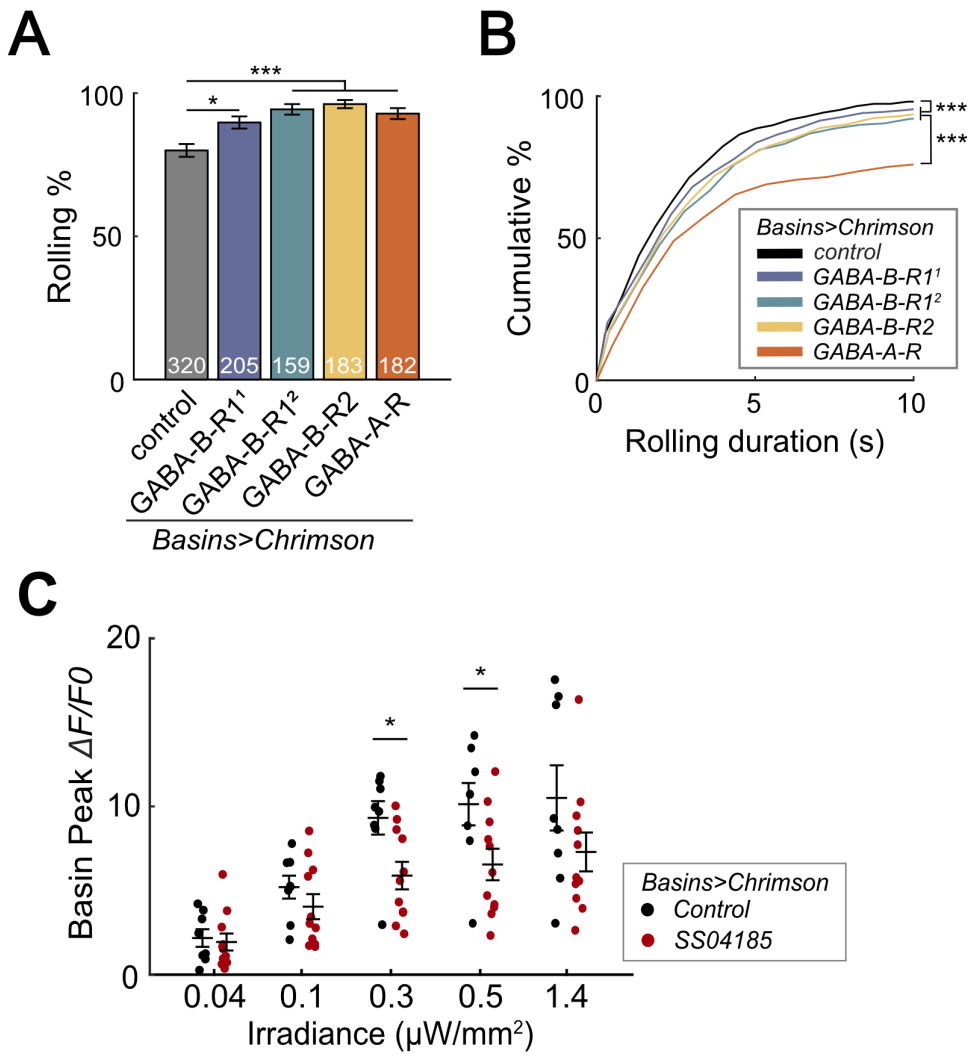

J. Zhu et al., Figure 7 - Figure supplement 1

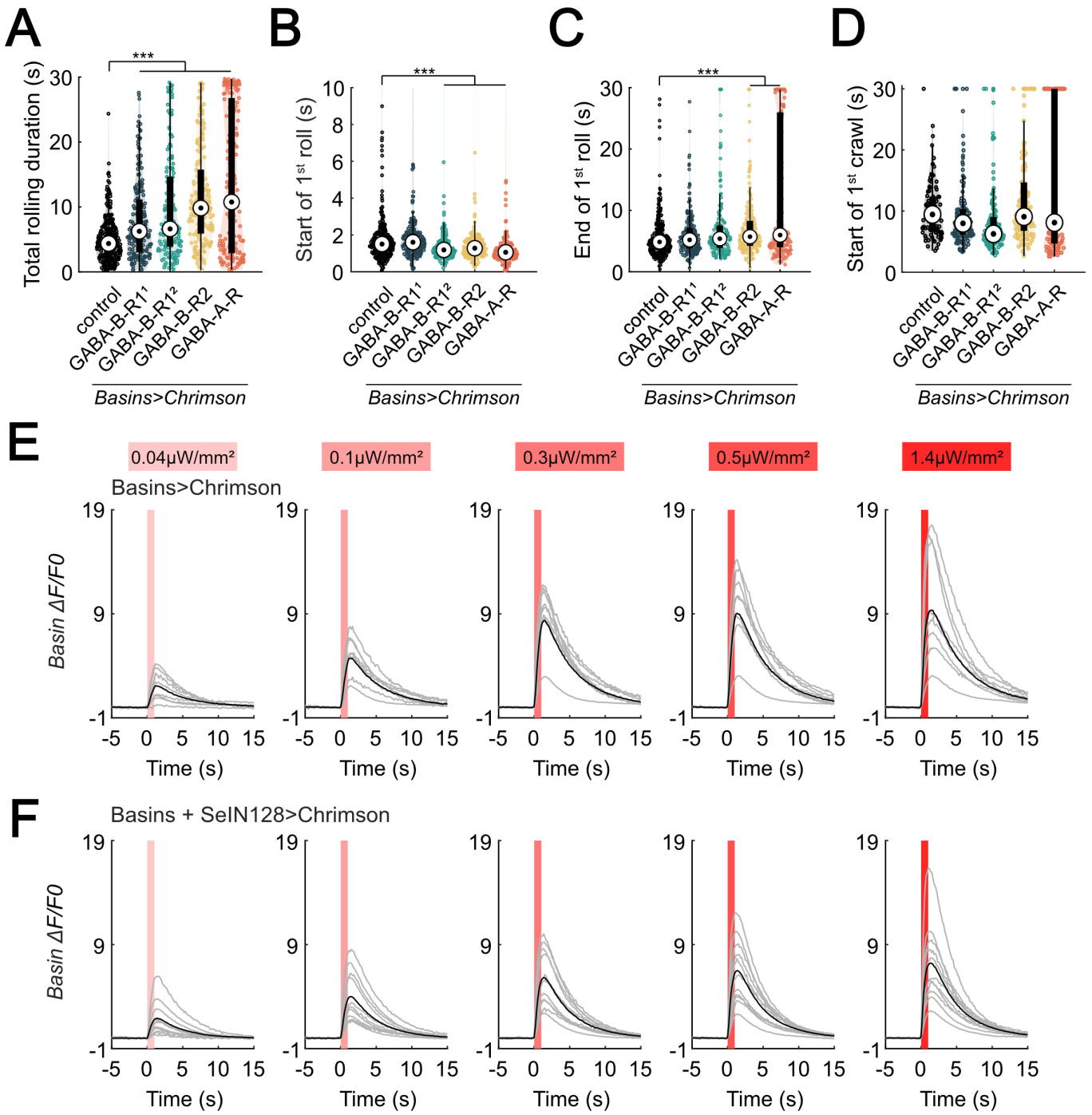

J. Zhu et al., Figure 8

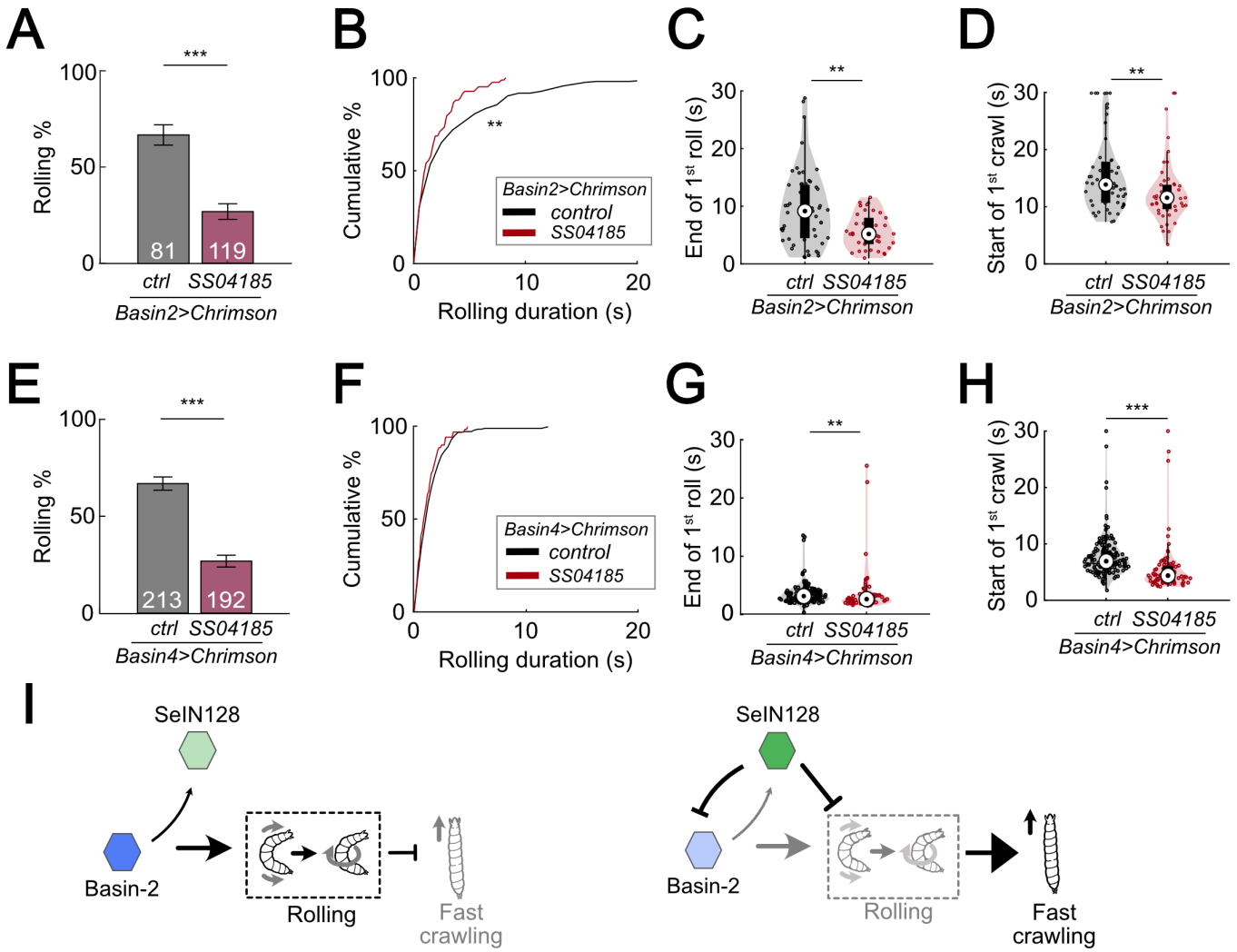
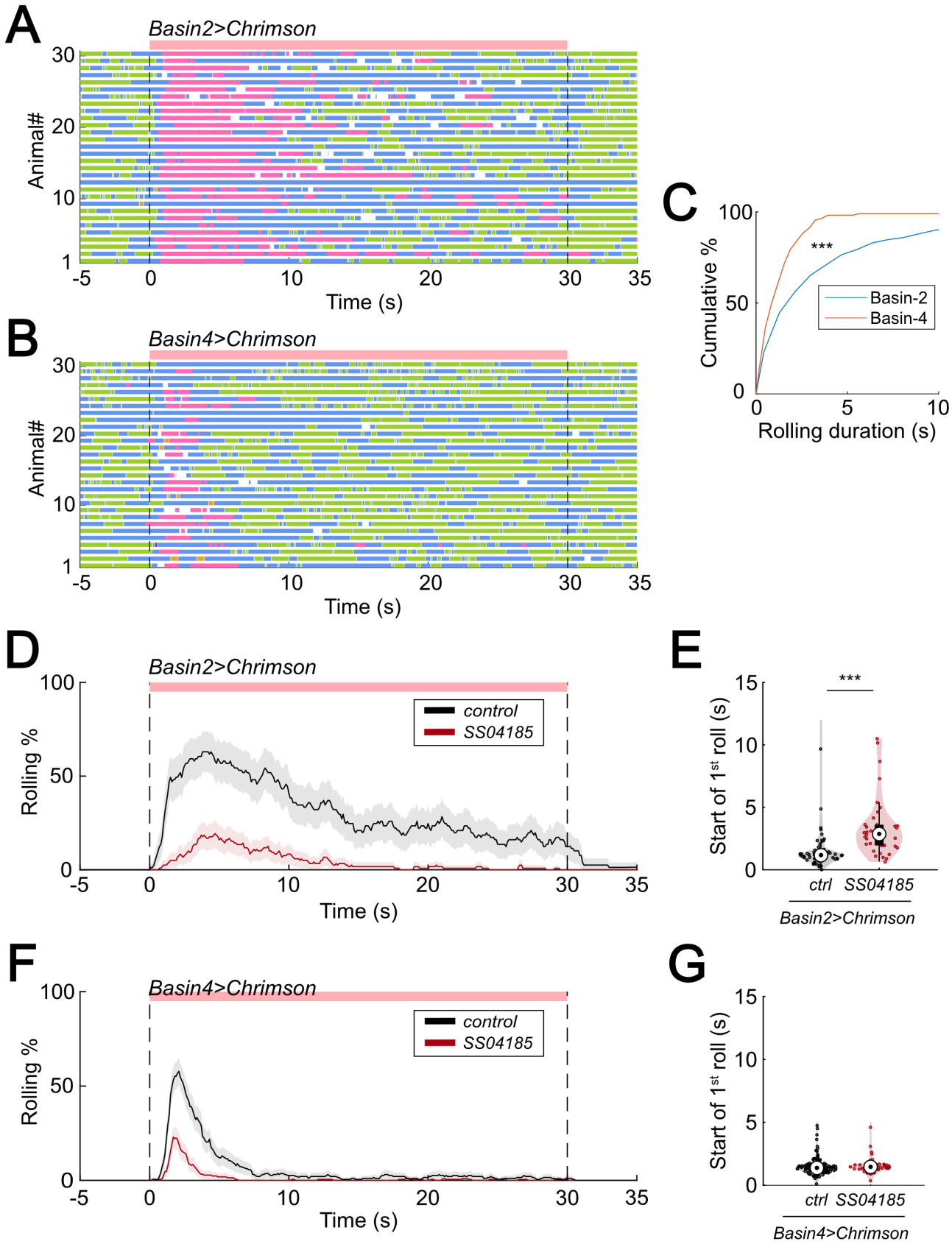
J. Zhu et al., Figure 8 - Figure supplement 1